ARTICLES
https://doi.org/10.1038/s41556-018-0084-5
nature cell biology

Loss of KLHL6 promotes diffuse large B-cell lymphoma growth and survival by stabilizing the mRNA decay factor roquin2

Jaewoo Choi[1,2], Kyutae Lee[1,2], Kristin Ingvarsdottir[3], Roberto Bonasio[3], Anita Saraf[4], Laurence Florens[4], Michael P. Washburn[4,5], Saber Tadros[6], Michael R. Green[6,7] and Luca Busino[1,2]*

Kelch-like protein 6 (*KLHL6*) is an uncharacterized gene mutated in diffuse large B-cell lymphoma (DLBCL). Here we report that KLHL6 assembles with cullin3 to form a functional cullin–RING ubiquitin ligase. Mutations in KLHL6 inhibit its ligase activity by disrupting the interaction with cullin3. Loss of KLHL6 favours DLBCL growth and survival both in vitro and in xenograft models. We further established that the mRNA decay factor roquin2 is a substrate of KLHL6. Degradation of roquin2 is dependent on B-cell receptor activation, and requires the integrity of the Tyr691 residue in roquin2 that is essential for its interaction with KLHL6. A non-degradable roquin2(Y691F) mutant requires its RNA-binding ability to phenocopy the effect of KLHL6 loss. Stabilization of roquin2 promotes mRNA decay of the tumour suppressor and NF-κB pathway inhibitor, tumour necrosis factor-α-inducible gene 3. Collectively, our findings uncover the tumour suppressing mechanism of KLHL6.

B-cell cancers hijack protein ubiquitylation and degradation pathways to promote growth and survival, as shown by the successful use of a proteasome inhibitor (bortezomib) and E3 ubiquitin ligase inhibitor (lenalinomide) as a treatment for multiple myeloma and mantle cell lymphoma[1]. Despite notable progress, much remains to be explored in the field of ubiquitin and the molecular mechanisms of tumorigenesis.

KLHL6 is a member of the bric-a-brac/tramtrack/broad-complex (BTB) domain family of proteins with a lymphoid tissue-restricted expression pattern[2,3]. Whole-genome and exome sequencing have revealed cancer-associated mutations in *KLHL6* in B-cell malignancies, including diffuse large B-cell lymphoma (DLBCL)[4–7]; however, the relevance of these mutations as well as the molecular function of KLHL6 remains unknown.

DLBCL is the most common type of lymphoid malignancies with two distinct molecular subtypes: activated B cell-like (ABC) and germinal centre B cell-like (GCB) lymphoma[8,9]. ABC-DLBCLs depend on hyperactivation of the inhibitor of IκB kinase (IKK) and the NF-κB transcription factor program for their proliferation and survival[10,11]. This is revealed by the frequent mutations in the BCR pathway, including activating mutations in positive (*CD79A*, *CD79B* and *CARD11*[12,13]) and inactivating mutations in negative (tumour necrosis factor-α-inducible gene 3, *TNFAIP3*[12–15]) NF-κB regulators. How KLHL6 contributes to the pathology of human DLBCL and whether it influences NF-κB activation are currently unknown.

Regulatory networks that promote cancer progression modulate gene expression at the level of mRNA stability[16,17]. The RNA-binding proteins roquin1 and roquin2 (hereafter roquin1 and roquin2) promote mRNA decay via recognition of stem–loop motifs in the 3′ untranslated region (UTR) of target mRNAs[18,19]. Through this recognition, roquins recruit the CCR4–CAF1–NOT complex, leading to mRNA deadenylation and subsequent destabilization[18–22]. In T cells, roquin proteins contribute to immune homeostasis by promoting the decay of inducible T-cell costimulator (ICOS). However, the role of roquin in B-cell cancers has not been investigated[18,23].

Here, we demonstrate that KLHL6 is an E3 ligase for roquin2. Cancer-associated mutations in KLHL6 inhibit its ubiquitin ligase activity and inactivation or loss of KLHL6 in ABC-DLBCL cells promotes cancer cell growth and survival through stabilization of roquin2 and subsequent decay of *TNFAIP3* mRNA. This study shows how ABC-DLBCL cells hijack the ubiquitin pathway to promote their proliferation via alteration of the mRNA decay process.

Results

KLHL6 mutations in human DLBCL abolish its catalytic function as cullin3-RING-ligase complex. Analysis of genomic databases of human patients with mature B-cell cancers revealed mutations in *KLHL6* in patients with DLBCL (http://cancergenome.nih.gov/ and refs [4–7]), chronic lymphocytic leukaemia[24] and multiple myeloma[25] (Fig. 1a). DLBCL cohorts displayed the highest rate of genetic mutations (Fig. 1a), which are similarly stratified among GCB-DLBCL, ABC-DLBCL and uncharacterized DLBCL (Fig. 1b). Most mutations in DLBCL are missense and monoallelic, with a low number of non-sense and frameshift mutations (Fig. 1c, Supplementary Table 1 and refs [4–7]). The majority of mutations clusters near and inside the BTB-domain of KLHL6 with mutational hotspots in Leu65 and Leu90 (Fig. 1c). Moreover, re-analysis of published single-nucleotide polymorphism (SNP) array data[26] revealed infrequent deletion of the *KLHL6* locus (Supplementary Fig. 1a), while approximately

[1]Department of Cancer Biology, University of Pennsylvania, Philadelphia, PA, USA. [2]Abramson Family Cancer Research Institute, Perelman School of Medicine, University of Pennsylvania, Philadelphia, PA, USA. [3]Epigenetics Institute, Department of Cell and Developmental Biology, University of Pennsylvania, Philadelphia, PA, USA. [4]The Stowers Institute of Medical Research, Kansas City, MO, USA. [5]Department of Pathology and Laboratory Medicine, The University of Kansas Medical Center, Kansas City, KS, USA. [6]Department of Lymphoma and Myeloma, University of Texas MD Anderson Cancer Center, Houston, TX, USA. [7]Department of Genomic Medicine, University of Texas MD Anderson Cancer Center, Houston, TX, USA.
*e-mail: businol@upenn.edu

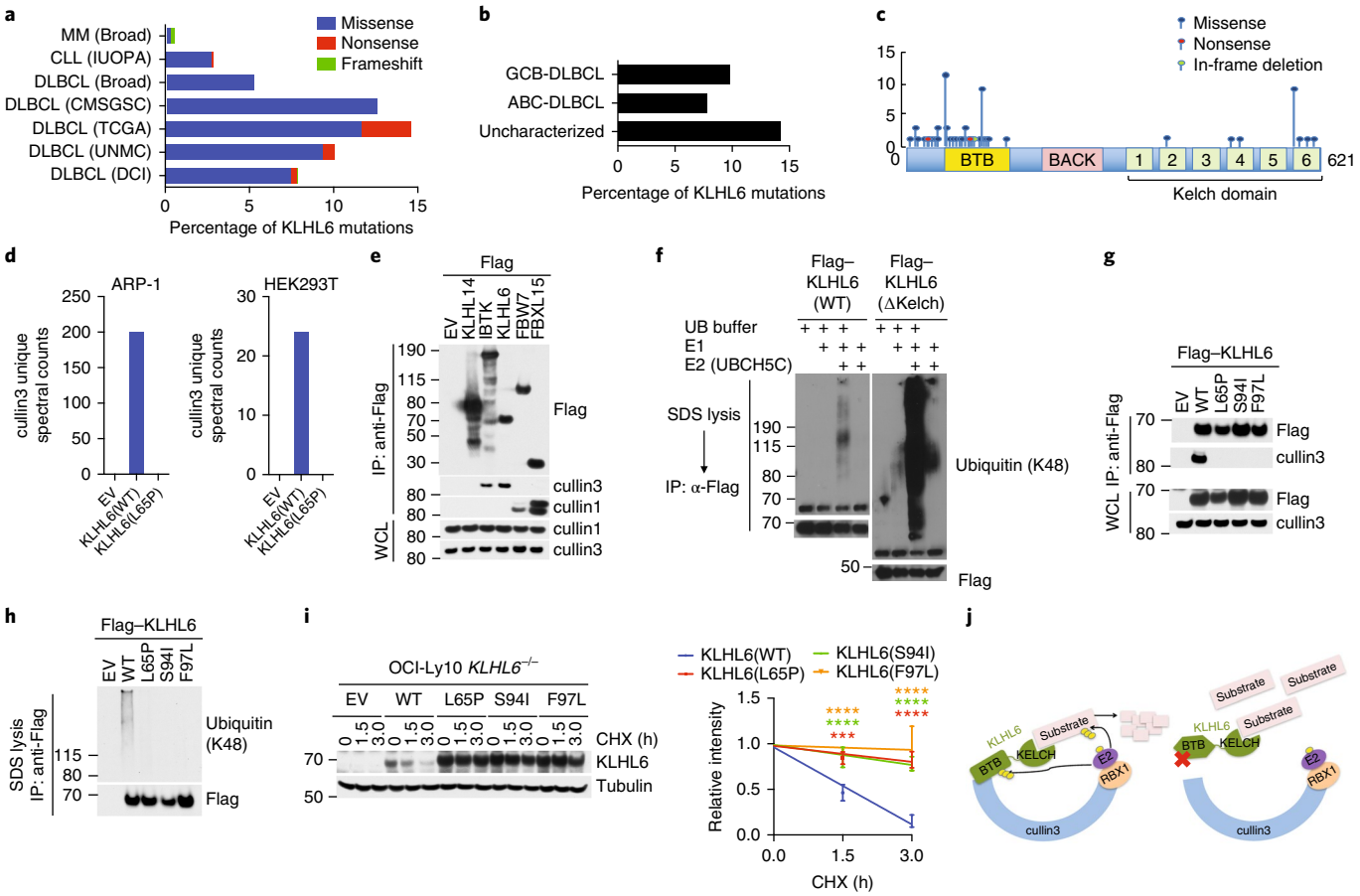

Fig. 1 | KLHL6 mutations in human DLBCL abolish its catalytic function as cullin3–RING–ligase. a, Percentage of *KLHL6* mutations in patients with DLBCL (University of Nebraska Medical Center (UNMC), $n=140$ patients; The Cancer Genome Atlas (TCGA), $n=48$; Canada's Michael Smith Genome Sciences Centre (CMSGSC), $n=96$; Broad Institute (Broad), $n=58$; Duke Cancer Institute (DCI), $n=1{,}001$), chronic lymphocytic leukaemia (CLL; Departamento de Bioquímica y Biología Molecular, Instituto Universitario de Oncología (IUOPA), $n=586$) and multiple myeloma (MM; Broad, $n=205$). **b**, Percentage of *KLHL6* mutations in DLBCL subtypes. Cohorts from UNMC and CMSGSC were pooled and sub-classified as ABC-DLBCL, GCB-DLBCL and uncharacterized DLBCL. **c**, Schematic representation of *KLHL6* mutations. BACK, BTB and C-terminal Kelch plant homeodomain. **d**, Proteomic analysis of KLHL6 complex. Spectral counts for cullin3 are shown. EV, empty vector. This analysis was performed once in HEK293T and ARP-1 cells. **e**, Immunoblot analysis of immunoprecipitated Flag-tagged E3 ligases in HEK293T cells. IP, immunoprecipitate; WCL, whole-cell lysates. **f**, In vitro ubiquitylation reaction of immunopurified Flag–KLHL6 and ΔKelch mutant (KLHL6 consisting only of the BTB-domain).Ubiquitin buffer reaction consists of Ubiquitin, E1, E2 (UBCH5C) and ATP. **g**, Immunoblot analysis of immunoprecipitated Flag-tagged wild-type (WT) KLHL6, BTB-domain mutant KLHL6 (L65P, S94I and F97L) or empty vector in HEK293T cells. **h**, In vitro ubiquitylation reaction of immunopurified wild-type and BTB-domain mutant (L65P, S94I and F97L) Flag–KLHL6. **i**, Left, immunoblot analysis of whole-cell lysates from GFP$^+$ OCI-Ly10 *KLHL6*$^{-/-}$ cells (clone-derived) retrovirally transduced with cDNAs encoding an empty vector, wild-type KLHL6 or BTB-domain mutant KLHL6 (L65P, S94I and F97L) and carrying a GFP marker. Cells were treated with cycloheximide (CHX) for the indicated times. Right, quantification of KLHL6 protein levels. Data are mean ± s.d., $n=3$ independent experiments, two-way ANOVA, $^{***}P \leq 0.001$; $^{****}P \leq 0.0001$. **j**, Schematic model of cullin3–RING–ligase (CRL3)–KLHL6 complex. Unprocessed scans of immunoblots in **e**–**i** are shown in Supplementary Fig. 8, and statistical source data and exact *P* values for **i** can be found in Supplementary Table 6. Unless otherwise noted, immunoblots are representative of three independent experiments.

6% of DLBCL tumours displayed lower expression of the *KLHL6* transcript (Supplementary Fig. 1b).

To understand the impact of these cancer-associated mutations, we compared the protein interactome of KLHL6(WT) to that of the cancer mutant KLHL6(L65P). Flag–KLHL6(WT) or Flag–KLHL6(L65P) complexes were immunopurified from two cell lines (HEK293T and ARP-1) and the tryptic digestion of each protein eluate was analysed by mass spectrometry (Supplementary Table 2). Unique spectral counts corresponding to cullin3 were identified in KLHL6(WT), but not in KLHL6(L65P), immunoprecipitates (Fig. 1d and Supplementary Table 2).

We validated our proteomic analysis via immunoprecipitation of KLHL6 with endogenous cullin3, but not cullin1, in HEK293T cells (Fig. 1e). By carrying out an in vitro ubiquitylation assay, we found that KLHL6 promoted self-ubiquitylation and, notably, its BTB-domain alone (KLHL6(ΔKelch)) was sufficient for catalysing self-polyubiquitylation to a greater degree (Fig. 1f). These data suggest that KLHL6 assembles a functional cullin3–RING–ligase (CRL3) complex[27] (Fig. 1j).

We then investigated the effect of DLBCL-associated BTB-domain mutations on KLHL6 ligase assembly and activity. All mutations tested (L65P, S94I, F97L) disrupted binding to cullin3 (Fig. 1g) and consequently led to a loss of self-polyubiquitylation in vitro (Fig. 1h). Correspondingly, the protein levels of BTB-domain KLHL6 mutants were remarkably high at steady state and displayed extended half-lives compared to those of wild-type KLHL6 (Fig. 1i), suggesting loss of KLHL6 self-ubiquitylation affects its turnover in cells.

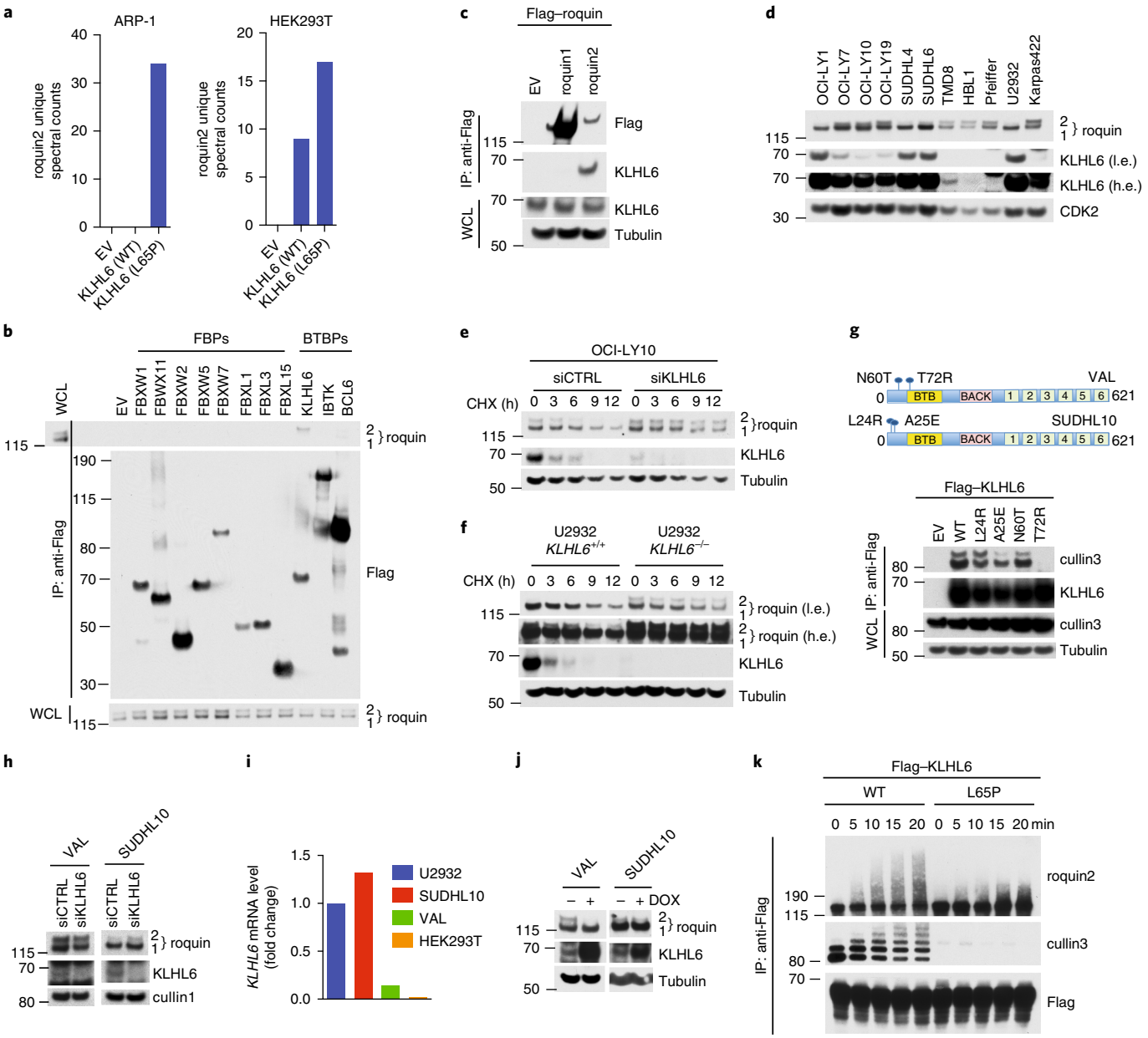

Fig. 2 | KLHL6 interacts and promotes ubiquitylation and degradation of roquin2. a, Proteomic analysis of KLHL6 immunoprecipitations. Spectral counts for roquin2 proteins are shown. The analysis was performed once in two different cell lines (HEK293T and ARP-1). **b**, Immunoblot analysis of immunoprecipitated Flag-tagged F-box proteins (FBPs) or BTB proteins (BTBPs) in HEK293T cells. Lane 1 shows whole-cell lysates from cells transfected with an empty vector. **c**, Immunoblot analysis of immunoprecipitated Flag–roquin1 or Flag–roquin2 in HEK293T cells. **d**, Immunoblot analysis of human DLBCL cell lysates. Low exposure (l.e.) and high exposure (h.e.) blots are shown. A representative blot from two independent experiments is shown. **e**, Immunoblot analysis of whole-cell lysates from OCI-LY10 cells electroporated with indicated short interfering RNAs (siRNAs) and treated with cycloheximide (CHX). Quantification and statistical analysis is shown in Supplementary Fig. 2d. **f**, *KLHL6*$^{+/+}$ and *KLHL6*$^{-/-}$ U2932 cells (clone-derived) were processed as in **e**. Low exposure (l.e.) and high exposure (h.e.) blots are shown. Quantification and statistical analysis is shown in Supplementary Fig. 2d. **g**, Top, schematic representation of KLHL6 protein displaying endogenous mutations in VAL and SUDHL10. Bottom, immunoblot analysis from immunoprecipitated Flag-tagged wild-type KLHL6, mutant KLHL6 (L24R, A25E, N60T and T72R) or empty vector in HEK293T cells. **h**, Immunoblot analysis of whole-cell lysates from VAL and SUDHL10 cells electroporated with siRNA scramble (siCTRL) or targeting *KLHL6* (siKLHL6). **i**, Analysis of level of *KLHL6* mRNA by quantitative PCR (qPCR). The value of the PCR product from U2932 cells was set to 1. A representative graph from two independent experiments is shown. **j**, Immunoblot analysis of whole-cell lysates from VAL and SUDHL10 cells stably expressing KLHL6 under a doxycycline (DOX) inducible promoter with a puryomycin cassette after 12 h of DOX treatment. **k**, In vitro ubiquitylation reaction of immunopurified Flag–KLHL6 and HA-roquin2. Unprocessed scans of immunoblots in **b**–**h**,**j**,**k** are shown in Supplementary Fig. 8, and source data for **i** can be found in Supplementary Table 6. Unless otherwise noted, immunoblots are representative of three independent experiments.

KLHL6 interacts with and promotes the ubiquitylation and degradation of roquin2. Because KLHL6(L65P) is unable to promote ubiquitylation, we reasoned that it might trap (that is, interact with but not ubiquitylate) substrates (Fig. 1j). By ranking proteins by the number of unique spectral counts, we identified roquin2 as a potential substrate (Fig. 2a and Supplementary Table 2).

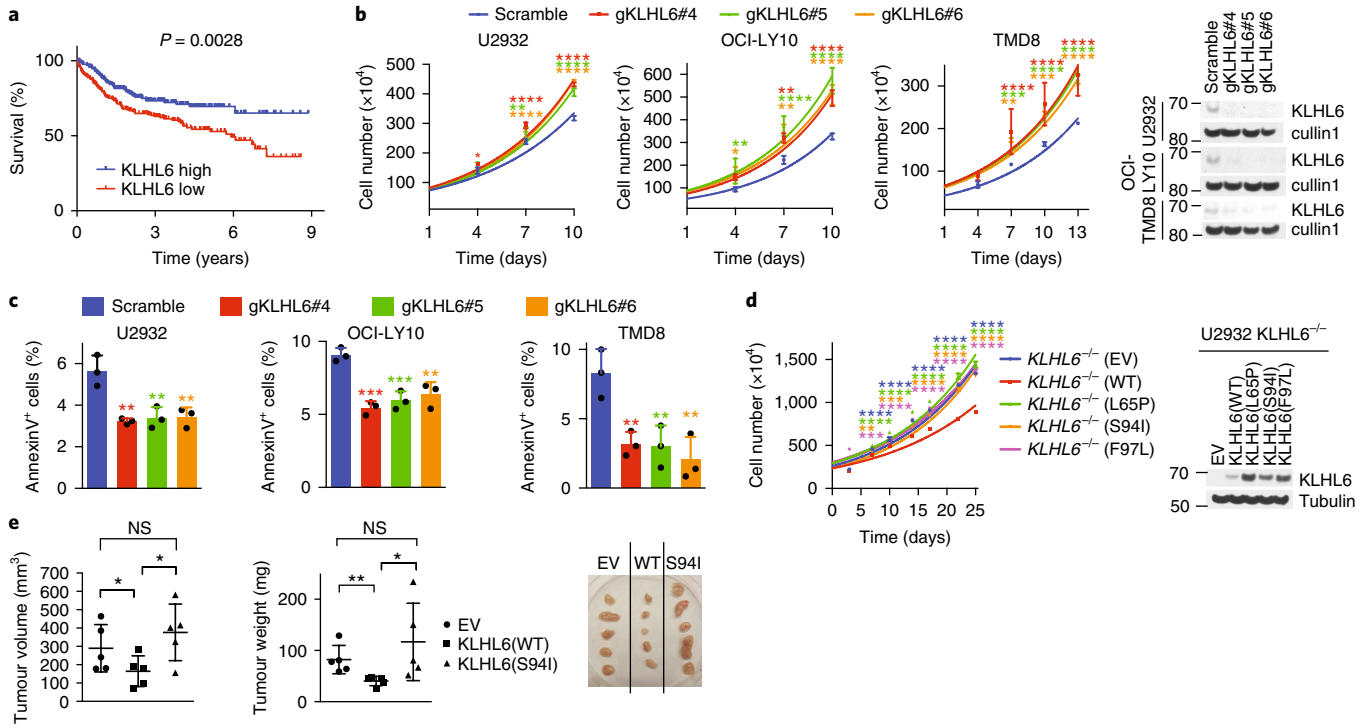

Fig. 3 | KLHL6 functions as a tumour suppressor in ABC-DLBCL by regulating its growth and survival. a, Kaplan–Meier analysis based on gene expression data for ABC-DLBCL tumours (GSE10846, GSE34171 and GSE3131239-41) is shown ($n=367$ patients). Censored subjects are indicated on the Kaplan-Meier curve as tick marks. Statistical analysis was performed using a log-rank (Mantel–Cox), two-sided test with 95% confidence interval. **b**, Left, cell counts of U2932, OCI-LY10 and TMD8 Cas9-expressing cells that expressed the indicated guide RNAs (gRNAs) and carrying a puromycin cassette. Data are mean ± s.d., $n=3$ independent experiments, two-way ANOVA, $^*P\leq0.05$; $^{**}P\leq0.01$; $^{***}P\leq0.001$; $^{****}P\leq0.0001$. Cells were grown in medium containing 1 μg ml^{-1} (U2932 and OCI-LY10) or 4 μg ml^{-1} (TMD8) of F(ab′)$_2$-IgM. Right, immunoblot analysis of whole-cell lysates. **c**, Apoptosis analysis of U2932, OCI-LY10 and TMD8 Cas9-expressing cells that expressed the indicated gRNAs and a GFP marker. Cells were grown as in **b**. Apoptosis was quantified based on GFP$^+$ and AnnexinV$^+$ cells. Data are mean ± s.d., $n=3$ independent experiments, one-way ANOVA, $^{**}P\leq0.01$; $^{***}P\leq0.001$. **d,** Left, cell counts of GFP-sorted U2932 *KLHL6*$^{-/-}$ (clone-derived) cells expressing empty vector, KLHL6(WT) or BTB-domain mutants (L65P, S94I and F97L) and a GFP marker. Data are mean ± s.d., $n=3$ independent experiments, two-way ANOVA, $^{**}P\leq0.01$; $^{***}P\leq0.001$; $^{****}P\leq0.0001$. Right, immunoblot analysis of whole-cell lysates. **e**, Xenograft experiments with GFP-sorted U2932 *KLHL6*$^{-/-}$ cells expressing an empty vector, KLHL6(WT) or KLHL6(S94I) and a GFP marker. Right, tumours at the experimental endpoint. Tumour volume (mean ± s.d., $n=5$ mice per group, one-way ANOVA, $^*P\leq0.05$; NS, not significant) and tumour weight (mean ± s.d., $n=5$ mice per group, one-tailed Student's *t*-test, $^*P\leq0.05$; $^{**}P\leq0.01$; NS, not significant) are shown in the left and middle, respectively. Unprocessed scans of immunoblots in **b**,**d** are shown in Supplementary Fig. 8, and statistical source data and exact *P* values for **a**–**e** can be found in Supplementary Table 6. Unless otherwise noted, immunoblots are representative of three independent experiments.

In agreement with our proteomic data, KLHL6 specifically co-immunoprecipitated endogenous roquin2 in HEK293T cells (Fig. 2b). The reciprocal co-immunoprecipitation experiments confirmed that roquin2, but not roquin1, is a KLHL6 interactor (Fig. 2c). This complex was also detectable at an endogenous level in DLBCL cells (Supplementary Fig. 2a). Importantly, interaction between KLHL6 and roquin2 required the intact Kelch domain in KLHL6 (Supplementary Fig. 2b), further supporting a substrate-like interaction[28].

In DLBCL cell lines, abundance of KLHL6 and roquin2 displayed an inverse correlation (Fig. 2d and Supplementary Fig. 2c). To investigate whether KLHL6 controls roquin2 protein levels, we assessed roquin2 protein turnover upon knockdown or knockout of KLHL6 in OCI-LY10 and U2932 cells, respectively. In both cases, downregulation of KLHL6 significantly extended the half-life of roquin2, but not that of roquin1 (Fig. 2e,f and Supplementary Fig. 2d).

Gain-of-function experiments showed that re-expression of KLHL6 in cell lines with low *KLHL6* expression (that is, HEK293T and HBL1 cells) downregulated roquin2 protein levels (Supplementary Fig. 2e). Moreover, BTB-domain mutants were incapable of inducing roquin2 downregulation (Supplementary Fig. 2f). Notably, co-expression of KLHL6(WT) along with BTB-domain mutants still promoted roquin2 degradation, suggesting that these mutations are not dominant negative (Supplementary Fig. 2g).

Next, we used B-cell lymphoma cell lines that have endogenous *KLHL6* mutations. VAL cells harbour two BTB-domain mutations: N60T and T72R (Fig. 2g). Binding analysis revealed that only the KLHL6(T72R) mutant lost interaction with cullin3 (Fig. 2g), whereas the KLHL6(N60T) mutant did not. Knockdown of KLHL6 in VAL cells did not result in roquin2 accumulation (Fig. 2h), whereas re-expression of KLHL6 induced roquin2 downregulation (Fig. 2j). In VAL cells, expression of *KLHL6* at the mRNA level was comparatively low (Fig. 2i). This suggests that VAL cells have one *KLHL6* allele that is inactivated by a mutation in the BTB-domain and additional downregulation of *KLHL6* mRNA. By contrast, mutations in *KLHL6* in SUDHL10 cells had no impact on KLHL6 function (Fig. 2g–j).

Last, to explore whether KLHL6 directly controls roquin2 ubiquitylation in vitro, we incubated immunopurified KLHL6–roquin2 complex with a ubiquitylation mix. High-molecular weight species of roquin2 were detected with the KLHL6(WT) complex, but not with KLHL6(L65P) (Fig. 2k). Correspondingly, ubiquitylation of roquin2 was abolished in *KLHL6*$^{-/-}$ cell lines in vivo (Supplementary Fig. 2h).

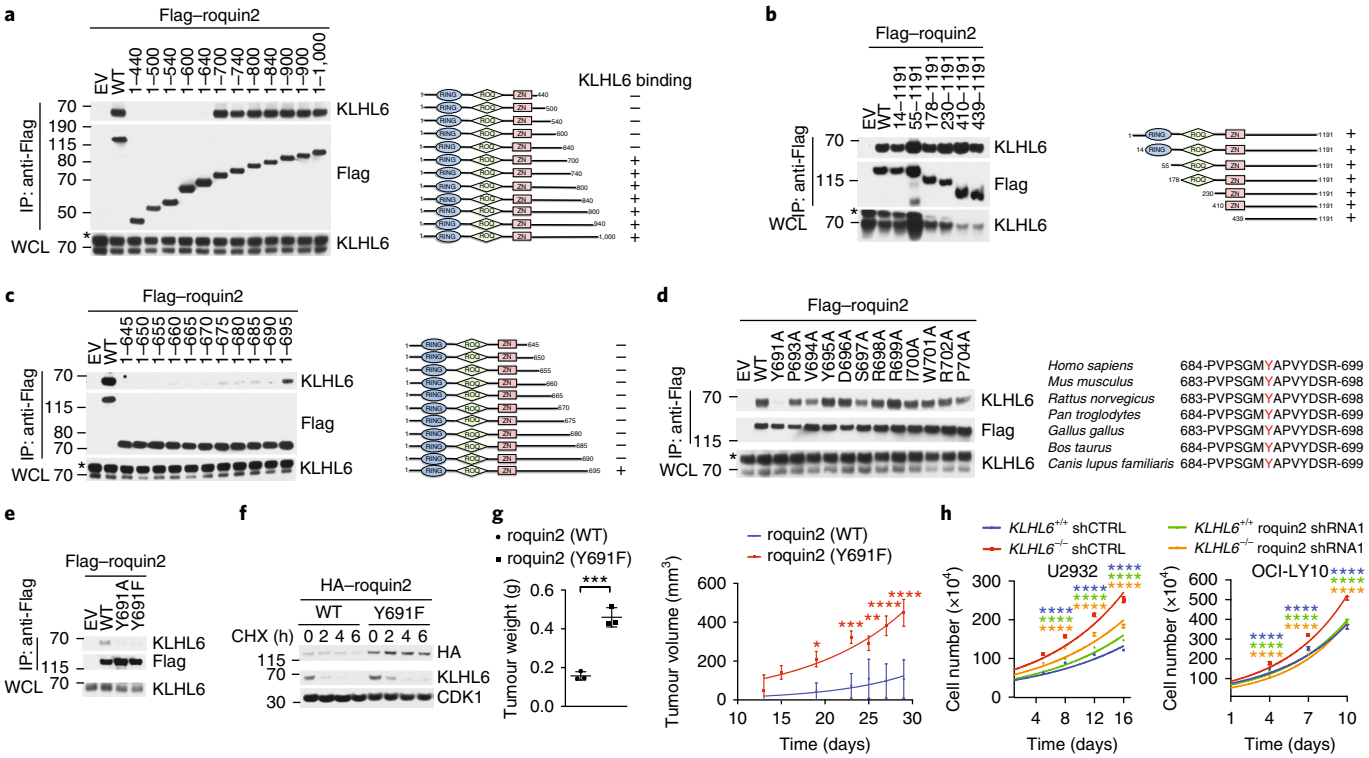

Fig. 4 | A non-degradable roquin2 mutant phenocopies loss of KLHL6. a Left, immunoblot analysis of immunoprecipitated Flag-tagged wild-type (WT) or mutant roquin2 in HEK293T cells stably expressing KLHL6. Right, a schematic representation of roquin2 mutants. roquin2 mutants that interact (+) or do not interact (−) with KLHL6 are shown. A representative blot from two independent experiments is shown. Asterisk indicates non-specific bands. **b**–**d**, Same as in **a**. **e**, Immunoblot analysis of immunoprecipitated Flag-tagged wild-type or mutant roquin2, as indicated, in HEK293T cells stably expressing KLHL6. **f**, Immunoblot analysis of whole-cell lysates from a DLBCL cell line, BJAB, retrovirally transduced with cDNAs encoding roquin2(WT) or roquin2(Y691F) carrying a puromycin cassette. Cells were treated with cycloheximide (CHX) for the indicated times. Quantification and statistical analysis are shown in Supplementary Fig. 4e. HA, haemagglutinin. **g**, Right, tumour volume from subcutaneously injected NOD/SCID/*Il2rγ*$^{-/-}$ (NSG) mice with U2932 cells stably expressing retroviruses encoding HA–roquin2(WT) or HA–roquin2(Y691F) carrying a puromycin cassette. Data are mean ± s.d., $n = 3$ mice per group, two-way ANOVA, $^{*}P \leq 0.05$; $^{**}P \leq 0.01$; $^{***}P \leq 0.001$; $^{****}P \leq 0.0001$. Left, tumour weight. Data are mean ± s.d., $n = 3$ mice per group, two-tailed Student's *t*-test, $^{***}P \leq 0.001$. **h**, Cell counts of GFP-sorted U2932 (left) or OCI-LY10 (right) *KLHL6*$^{+/+}$ and *KLHL6*$^{-/-}$ (clone-derived) cells infected with scramble shRNA(shCTRL) or shRNA targeting roquin2 (roquin2, shRNA1 or shRNA2) carrying a GFP marker. GFP^{+} cells were grown in medium containing 1 μg ml^{-1} of F(ab′)$_2$-IgM. Data are mean ± s.d., $n = 3$ independent experiments, two-way ANOVA, $^{****}P \leq 0.0001$. Unprocessed scans of immunoblots in **a**–**f** are shown in Supplementary Fig. 8, and statistical source data and exact *P* values for **g**,**h** can be found in Supplementary Table 6. Unless otherwise noted, immunoblots are representative of three independent experiments.

KLHL6 functions as a tumour suppressor in ABC-DLBCL by regulating its growth and survival. Although mutations in *KLHL6* occur at a similar rate in GCB- and ABC-DLBCL (Fig. 1b), low *KLHL6* expression correlated with a significantly poorer survival in ABC-DLBCL patients (Fig. 3a) as previously reported[29,30].

To assess the biological effect of *KLHL6* loss in ABC-DLBCL lines, we infected Cas9-expressing U2932, OCI-LY10 and TMD8 cells with lentiviruses encoding three different guide RNAs (gRNAs) targeting the *KLHL6* gene locus. Ablation of *KLHL6* resulted in an increase in cell proliferation and a decrease in apoptosis (Fig. 3b,c). This effect was confirmed in three-dimensional cultures as measured by a larger number and size of colonies (Supplementary Fig. 3a,b). To rule out the possible off-target effects of gRNAs, we used short hairpin RNA (shRNA)-mediated knockdown of *KLHL6* in U2932 and OCI-LY10 and observed similar results (Supplementary Fig. 3c–f).

To investigate the role of cancer mutations in cell growth, we re-expressed KLHL6(WT), KLHL6 BTB-domain mutants or an empty vector (EV) in a clonally derived U2932 *KLHL6*$^{-/-}$ cell line (Fig. 3d). Whereas re-expression of KLHL6(WT) decreased cell proliferation, expression of KLHL6 BTB-domain mutants phenocopied loss of *KLHL6*, confirming that these mutations resulted in loss of function. In xenograft models, expression of KLHL6(WT) decreased tumour burden whereas expression of KLHL6(S94I) led to a similar tumour burden compared to tumours generated from *KLHL6*$^{-/-}$ cells expressing the empty vector (Fig. 3e).

A non-degradable roquin2 mutant phenocopies loss of KLHL6. We mapped the KLHL6 binding motif in roquin2. By performing mutagenesis experiments, we identified that a region in roquin2 between amino acids 640 and 700 was necessary for the interaction with KLHL6 (Fig. 4a,b). More refined deletions narrowed the interaction domain between amino acids 690 and 695 (Fig. 4c). Alanine scanning mutagenesis of the individual residues surrounding the 691–704 region revealed that a conserved tyrosine residue, in position 691, was required for KLHL6–roquin2 interaction (Fig. 4d). In vitro binding assays confirmed that a roquin2 peptide consisting of residues 686–700 directly interacts with KLHL6 (Supplementary Fig. 4a–d). Mutating Tyr691 to alanine or phenylalanine impaired the ability of roquin2 to co-immunoprecipitate with KLHL6 in vivo and in vitro (Fig. 4e and Supplementary Fig. 4c), suggesting that the integrity of the tyrosine hydroxyl group is critical for the KLHL6 interaction.

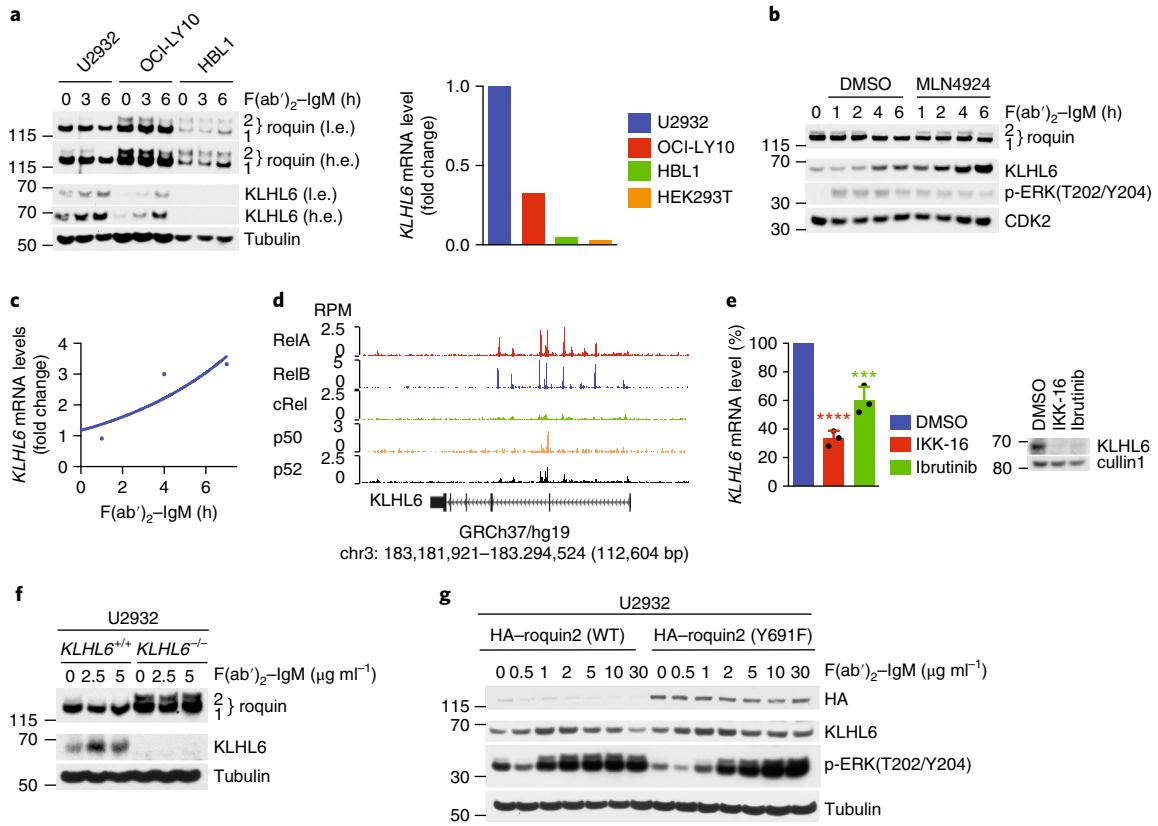

Fig. 5 | KLHL6 is a BCR/NF-κB target gene that links roquin2 degradation to BCR signaling. a, Left, immunoblot analysis of whole-cell lysates from OCI-LY10, U2932 and HBL1 cells stimulated with 10 μg ml^{-1} F(ab′)$_2$–IgM for 3 and 6 h. Low exposure (l.e.) and high exposure (h.e.) blots are shown. Right, level of *KLHL6* mRNA analysed by qPCR. The value of the PCR product from U2932 was set to 1. A representative graph from two independent experiments is shown. **b**, Immunoblot analysis of whole-cell lysates from U2932 cells treated with 10 μg ml^{-1} of F(ab′)$_2$–IgM for the indicated times. Where indicated, cells were pre-treated with 5 μM MLN4924 for 1 h. p-ERK, phosphorylated ERK. **c**, Analysis of level of *KLHL6* mRNA by qPCR in U2932 cells treated with 10 μg ml^{-1} of F(ab′)$_2$–IgM for the indicated times. A representative graph from two independent experiments is shown. The value of the PCR product without treatment was set to 1. **d**, Visualization of ChIP-seq peaks using the University of California Santa Cruz (UCSD) Genome browser (GEO series accession GSE55105). RPM, reads per million mapped. **e**, Left, same as in **c** except that U2932 cells were treated with DMSO, 10 μM of IKK inhibitor (IKK-16) or 5 μM of BTK inhibitor (ibrutinib) for 6 h. The value for the PCR product without treatment (DMSO) was set to 100%. Data are mean ± s.d., $n = 3$ independent experiments, one-way ANOVA, $^{***}P \leq 0.001$; $^{****}P \leq 0.0001$. Right, immunoblot analysis of whole-cell lysates for the indicated proteins. **f**, Immunoblot analysis of whole-cell lysates from U2932 *KLHL6*$^{+/+}$ and *KLHL6*$^{-/-}$ (clone-derived) cells treated with increasing concentrations of F(ab′)$_2$–IgM for 6 h. **g**, Immunoblot analysis of whole-cell lysates from U2932 cells stably expressing HA-roquin2(WT) or HA-roquin2(Y691F) treated with F(ab′)$_2$–IgM for 6 h. Unprocessed scans of immunoblots in **a**,**b**,**e**,**f**,**g** are shown in Supplementary Fig. 8, and source data for **a**,**c** and statistical source data and exact *P* values for **e** can be found in Supplementary Table 6. Unless otherwise noted, immunoblots are representative of three independent experiments.

We retrovirally transduced BJAB with roquin2(WT) or roquin2(Y691F) to investigate whether Tyr691 controls roquin2 stability in DLBCL cells. roquin2(Y691F) displayed increased protein levels at steady state as well as an increased half-life compared to roquin2(WT) (Fig. 4f and Supplementary Fig. 4e). Furthermore, KLHL6(WT) effectively downregulated protein levels of roquin2(WT), but not those of roquin2(Y691F) (Supplementary Fig. 4f). The KLHL6 BTB-domain mutant (KLHL6(L65P)) had no effect on protein levels of roquin2(WT) and roquin2(Y691F) (Supplementary Fig. 4f).

Next, we analysed the effect of roquin2 stabilization on DLBCL growth. Expression of the non-degradable roquin2(Y691F) mutant increased tumour burden as monitored by tumour volume and weight at the experimental endpoint (Fig. 4g). This effect was not an artifact of overexpression because the levels of roquin2(Y691F) were comparable to those of endogenous roquin2 in *KLHL6*$^{-/-}$ cells (Supplementary Fig. 4g). Moreover, knockdown of roquin2 impaired the cell growth advantage of *KLHL6*$^{-/-}$ U2932 and OCI-LY10 cells (Fig. 4h and Supplementary Fig. 4h,i). Importantly, loss of roquin2 increased toxicity of *KLHL6*$^{-/-}$ cells preferentially (Supplementary Fig. 4h), suggesting that loss of *KLHL6* promotes cell proliferation in a roquin2-dependent manner.

KLHL6 is a BCR/NF-κB target gene that links roquin2 degradation to BCR signaling. KLHL6 is a member of the B-cell receptor (BCR) signalosome[31] and is induced upon antigen stimulation in the germinal centre[3]. Thus, we investigated whether mRNA and protein levels of KLHL6 and roquin2 were affected by BCR stimulation. First, we found that ABC-DLBCL cells predominantly expressed an IgM–BCR as opposed to GCB-DLBCL cells, which are positive for IgG–BCR[32] (Supplementary Fig. 5a). Subsequently, we analysed levels of KLHL6 and roquin2 in IgM-positive ABC-DLBCL cell lines (U2932, OCI-LY10 and HBL1) (Fig. 5a). BCR stimulation using fragment affinity-purified antibody F(ab′)$_2$–IgM induced upregulation of KLHL6 and a corresponding downregulation of roquin2 protein levels in OCI-LY10 and U2932 cells, but not in HBL1 cells (a human cell line with low levels of both *KLHL6* mRNA and KLHL6 protein (Fig. 5a)).

To demonstrate that BCR-dependent downregulation of roquin2 protein depends on CRLs, we pre-treated U2932 cells with

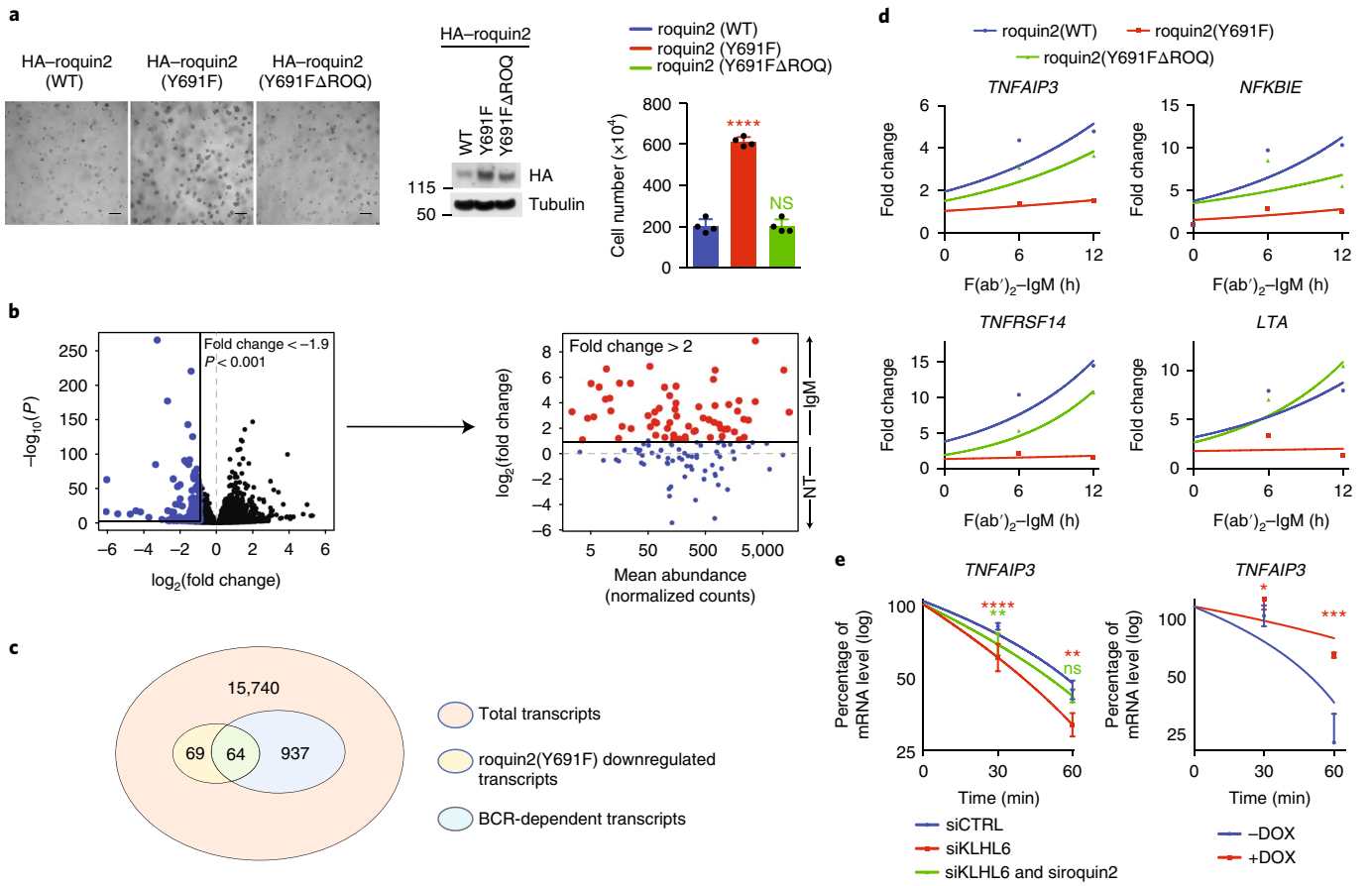

Fig. 6 | Stabilization of roquin2 downregulates BCR responsive genes. a, Left, representative images of U2932 cells expressing HA–roquin2(WT), HA–roquin2(Y691F) or HA–roquin2(Y691FΔROQ) with puromycin cassette plated into a Matrigel. Middle, immunoblot analysis of whole-cell lysates. Right, cell counts from the Matrigel. Data are mean ± s.d., $n = 4$ independent experiments, one-way ANOVA, $^{****}P \leq 0.0001$, NS, not significant. Scale bars, 150 µm. **b**, Left, volcano plot showing downregulated mRNAs (blue) in U2932 cells expressing roquin2(Y691F) versus roquin2(WT) after 12 h treatment with 10 µg ml^{-1} of F(ab′)$_2$–IgM ($\log_2$(fold change) < −0.9). Right, downregulated mRNAs were further plotted in an M (log ratio) and A (mean average), MA plot. The mRNAs upregulated on treatment with F(ab′)$_2$–IgM in cells expressing roquin2(WT) ($\log_2$(fold change) > 1) are shown in red. NT, not treated. $n = 3$ independent experiments, DEseq2, $P < 0.001$. **c**, Venn diagram showing the overlap between genes downregulated by expression of roquin2(Y691F) and BCR responsive genes. **d**, qPCR analysis of the indicated mRNAs in U2932 cells expressing HA–roquin2(WT), HA–roquin2(Y691F) or HA–roquin2(Y691FΔROQ) treated with 10 µg ml^{-1} of F(ab′)$_2$–IgM for indicated times. The value of the PCR product at time 0 h was set to 1 for each condition. A representative graph from two independent experiments is shown. **e**, Left, qPCR analysis of *TNFAIP3* mRNA in U2932 cells electroporated with indicated siRNAs and treated with actinomycin D for the indicated times. The value of the PCR product at time 0 h was set to 100%. Data are mean ± s.d., $n = 3$ independent experiments, two-way ANOVA, $^{**}P \leq 0.01$, $^{****}P \leq 0.0001$, NS, not significant. Right, same analysis was performed in VAL cells expressing *KLHL6* under a DOX-inducible promoter. Cells were pre-treated with DOX for 12 h and actinomycin D for the indicated times. Data are mean ± s.d., $n = 3$ independent experiments, two-way ANOVA, $^{*}P \leq 0.05$; $^{***}P \leq 0.001$. Unprocessed scans of immunoblots in **a** are shown in Supplementary Fig. 8, and source data for **d** and statistical source data and exact *P* values for **a**,**e** and **b** can be found in Supplementary Tables 6 and 3, respectively. Unless otherwise noted, immunoblots are representative of three independent experiments.

MLN4924, a NEDD8-activating enzyme inhibitor that blocks cullin neddylation[33]. MLN4924 treatment rescued roquin2 downregulation induced by BCR crosslinking, suggesting that a functional CRL complex is required to promote roquin2 degradation (Fig. 5b). Notably, BCR stimulation induced KLHL6 upregulation both at transcriptional and protein levels (Fig. 5a–c).

Because BCR signaling converges on NF-κB activation[10], we investigated whether *KLHL6* is an NF-κB target gene. Analysis of chromatin immunprecipitation followed by sequencing (ChIP–seq) datasets of NF-κB factors[34] revealed enrichment of p50, p52, V-Rel avian reticuloendotheliosis viral oncogene homologue A (RelA) and B (RelB) at the *KLHL6* gene locus (Fig. 5d). Correspondingly, treatment of cells with an IKK or a BTK inhibitor (ibrutinib)[13], resulted in a downregulation of KLHL6 both at mRNA and protein levels (Fig. 5e). Interestingly, a reduced sensitivity of *KLHL6*$^{-/-}$ cells to ibrutinib was observed (Supplementary Fig. 5b).

BCR-induced roquin2 degradation was impaired in *KLHL6*$^{-/-}$ (Fig. 5f) and *KLHL6*-knockdown cells (Supplementary Fig. 5c,d). Correspondingly, whereas exogenous roquin2(WT) was degraded in a dose-dependent manner upon BCR stimulation, roquin2(Y691F) mutant was not affected (Fig. 5g), supporting BCR signaling promotes roquin2 degradation in a KLHL6-dependent manner.

Stabilization of roquin2 downregulates BCR responsive genes. To investigate whether the pro-proliferative effect of the non-degradable roquin2(Y691F) mutant depends on its RNA binding ability, we generated a double mutant roquin2(Y691FΔROQ) that lacked the ROQ domain. Notably, deletion of the ROQ domain abolished the growth advantage induced by roquin2(Y691F) expression (Fig. 6a).

Next, we investigated whether misregulation of roquin2 degradation would result in a deregulation of the BCR transcriptional

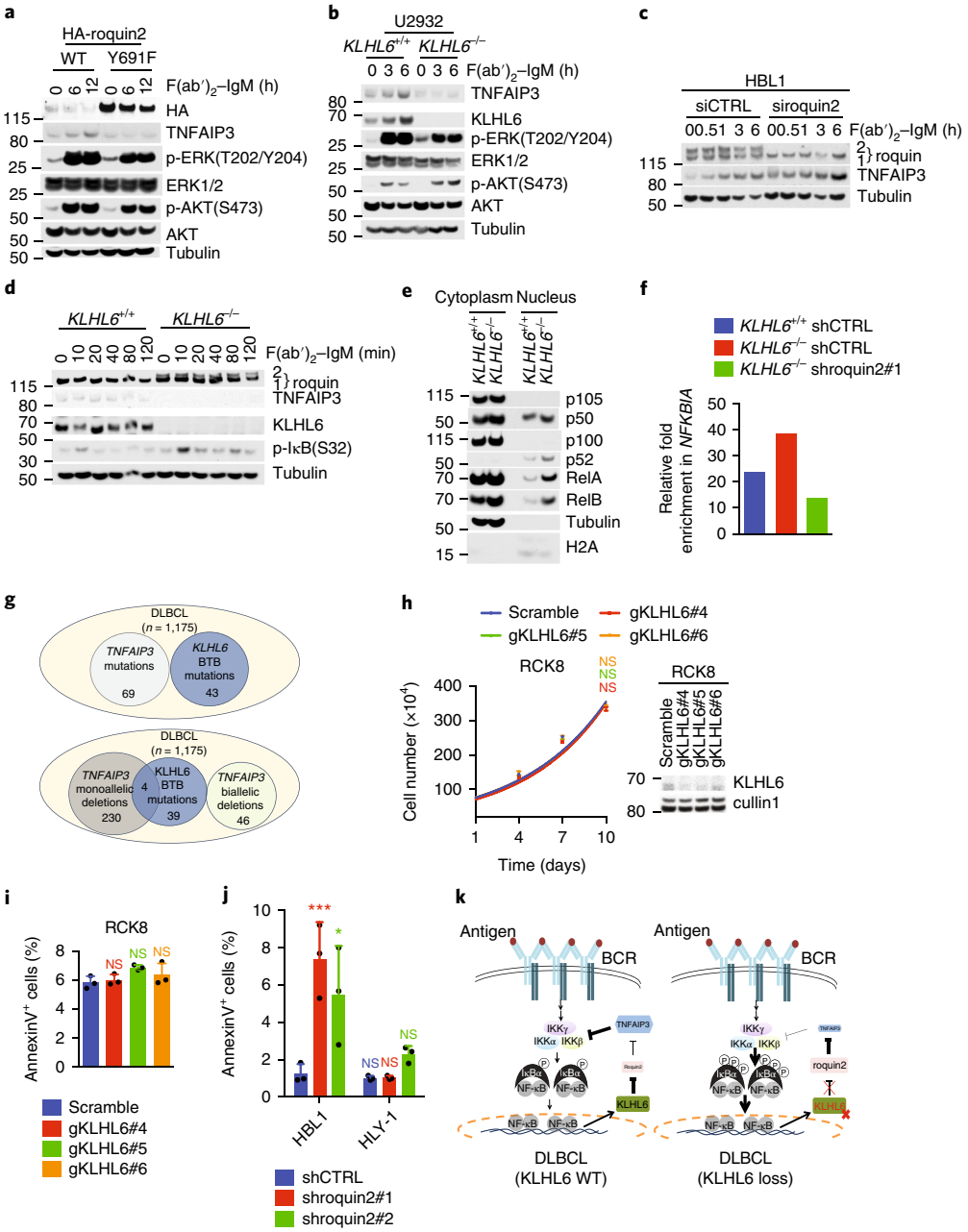

Fig. 7 | The KLHL6–roquin2 axis controls NF-κB activation. a, Immunoblot analysis of whole-cell lysates from U2932 cells expressing HA–roquin2(WT) or HA–roquin2(Y691F) treated with 10 μg ml^{-1} of F(ab′)$_2$–IgM for the indicated times. p-AKT, phosphorylated AKT. **b**, Immunoblot analysis of whole-cell lysates from U2932 *KLHL6*$^{+/+}$ or *KLHL6*$^{-/-}$ cells (clone-derived) treated with 10 μg ml^{-1} of F(ab′)$_2$–IgM for the indicated times. **c**, Immunoblot analysis of whole-cell lysates from HBL1 cells electroporated with indicated siRNAs and treated as in **a** for the indicated times. **d**, Immunoblot analysis of whole-cell lysates from U2932 *KLHL6*$^{+/+}$ or *KLHL6*$^{-/-}$ cells (clone-derived) treated with 10 μg ml^{-1} of F(ab′)$_2$–IgM for the indicated times. p-IκB, phosphorylated IκB. **e**, Immunoblot analysis of fractionated U2932 *KLHL6*$^{+/+}$ or *KLHL6*$^{-/-}$ (clone-derived) cells. **f**, RelA ChIP–qPCR for the *NFBKIA* promoter in U2932 *KLHL6*$^{+/+}$, *KLHL6*$^{-/-}$ or *KLHL6*$^{-/-}$ cells infected with indicated shRNAs. Data are displayed as fold enrichment relative to IgG control. A representative graph from two independent experiments is shown. **g**, Overlap of BTB-associated mutations in *KLHL6* with *TNFAIP3* alterations in DLBCLs. Top, tumours sequenced at UNMC[6] and DCI[7] (n = 1,175) with deleterious mutations in the BTB-domain of *KLHL6* and *TNFAIP3* mutations. Bottom, the *TNFAIP3* subset is shown as biallelic and monoallelic deletions. **h**, Left, cell counts of GFP-sorted RCK8 cells expressing Cas9, the indicated gRNAs and a GFP marker. Cells were grown in medium containing 1 μg ml^{-1} of F(ab′)$_2$–IgM. Data are mean ± s.d., n = 3 independent experiments, two-way ANOVA, NS, not significant. Right, immunoblot analysis of whole-cell lysates. **i**, Apoptosis analysis of cells from **h**. Data are mean ± s.d., n = 3 independent experiments, one-way ANOVA, NS, not significant. **j**, The percentage of GFP$^+$ and AnnexinV$^+$ HBL1 and HLY-1 cells expressing the indicated shRNAs. Data are mean ± s.d., n = 3 independent experiments, one-way ANOVA, $^*P \leq 0.05$; $^{***}P \leq 0.001$, NS, not significant. **k**, Model of KLHL6–roquin2 axis in ABC-DLBCL. Unprocessed scans of immunoblots in **a**–**e**,**h** are shown in Supplementary Fig. 8, and source data for **f** and statistical source data for **h**–**j** and exact P values for **j** can be found in Supplementary Table 6. Unless otherwise noted, immunoblots are representative of three independent experiments.

program. We measured differential gene expression in U2932 cells expressing roquin2(WT) or roquin2(Y691F) upon BCR ligation via RNA-seq (Fig. 6b and Supplementary Table 3). Pairwise comparison revealed that 133 mRNAs were significantly downregulated

in roquin2(Y691F)-expressing cells compared to roquin2(WT). Of these 133 mRNAs, 64 overlapped with BCR-responsive genes defined as those with at least a twofold upregulation in expression upon BCR stimulation in cells expressing roquin2(WT) (Fig. 6b,c). These 64 genes represented BCR-responsive genes that failed to be upregulated upon BCR stimulation in the presence of a non-degradable roquin2 mutant.

Gene ontology enrichment analysis (Supplementary Fig. 6a and Supplementary Table 4) revealed that roquin2-regulated genes are involved in immune and inflammatory responses and implicated as regulators of the NF-κB pathway and lymphoid tumour suppressors (for example, *TNF*, *NFKBIE*, *TNFAIP3*, *LTA* and *TNFRSF14*.)[14,35–38]. To identify targets relevant to DLBCL biology, we ranked these genes by the percentage of genetic alterations in human DLBCL (TCGA (http://cancergenome.nih.gov/)) and the base mean expression in our RNA-seq analysis (Supplementary Fig. 6b and Supplementary Table 3). We validated the top 11 candidates in a secondary screen and found that 7 of these genese were dependent on a functional ROQ domain (Supplementary Fig. 6b,c).

Amongst these targets, we focused on *TNFAIP3*, because it is frequently inactivated in ABC-DLBCLs[12–15] and is a direct target of the roquin proteins[19]. We found that *TNFAIP3* was upregulated upon BCR stimulation, consistent with its function as a negative regulator of the NF-κB[39] (Fig. 6d). This response was abolished in cells expressing roquin2(Y691F), suggesting that stabilization of roquin2 contributes to a reduction in *TNFAIP3* mRNA levels during BCR signaling. This effect was rescued partially in cells expressing roquin2(Y691FΔROQ), as a build-up of *TNFAIP3* mRNA levels was observed. Notably, other NF-κB target genes (*NFKBIE* and *LTA*) and the tumour suppressor gene *TNFRSF14* displayed a similar pattern.

Lastly, we investigated whether the KLHL6–roquin2 axis directly controls *TNFAIP3* mRNA stability. Ablation of KLHL6 shortened the half-life of *TNFAIP3*, which was partially rescued by concomitant ablation of roquin2 (Fig. 6e). Re-expression of KLHL6(WT) in VAL cells, which carry endogenous mutations in the BTB-domain, also increased the half-life of *TNFAIP3* (Fig. 6e).

The KLHL6–roquin2 axis controls NF-κB activation. Because KLHL6 regulates *TNFAIP3* mRNA levels, we hypothesized that loss of *KLHL6* would lead to increased NF-κB activation in ABC-DLBCL. First, we investigated whether the *TNFAIP3* transcriptional changes would reflect similar changes in protein levels. BCR-dependent degradation of roquin2(WT) inversely correlated with the upregulation of TNFAIP3 levels, which was reduced in cells stably expressing roquin2(Y691F) (Fig. 7a). Correspondingly, TNFAIP3 protein levels were downregulated in *KLHL6*$^{-/-}$ cells, both at steady state and in response to BCR stimulation (Fig. 7b). Knockdown of roquin2 in U2932 *KLHL6*$^{-/-}$ cells rescued TNFAIP3 levels similar to those of *KLHL6*$^{+/+}$ cells (Supplementary Fig. 7a). Likewise, depletion of roquin2 more robustly upregulated TNFAIP3 protein levels in HBL1 cells (Fig. 7c). Correspondingly, re-expression of KLHL6(WT) in U2932 *KLHL6*$^{-/-}$ cells increased TNFAIP3 levels (Supplementary Fig. 7b).

Next, we investigated whether loss of *KLHL6* resulted in increased IKK activation. The amount of IκBα phosphorylation upon BCR stimulation was higher in *KLHL6*$^{-/-}$ cells, suggesting increased IKK activity (Fig. 7d). Importantly, the increase in phosphorylation was reduced after re-expression of KLHL6(WT) (Supplementary Fig. 7c). We also detected an increase in the nuclear translocation of the NF-κB transcriptional factors in *KLHL6*$^{-/-}$ cells (Fig. 7e), which was partially mitigated by the concomitant knockdown of roquin2 (Supplementary Fig. 7d). Moreover, ablation of KLHL6 increased RelA DNA-binding at the *NFKBIA* promoter, an effect reversed by simultaneous knockdown of roquin2 (Fig. 7f).

We analysed the mutual exclusivity of BTB-associated *KLHL6* mutations with *TNAFAIP3* alterations in DLBCL patients. Deleterious mutations in the *KLHL6* BTB-domain showed no overlap with *TNFAIP3* biallelic deletion or mutation (Fig. 7g and Supplementary Fig. 7e). Using a weighted test[40], we found exclusivity with a trend toward significance ($P=0.085$, Supplementary Table 5). Instead, four mutations in the BTB-domain had a coincident monoallelic deletion in *TNFAIP3*, suggesting that these mutations might confer additional NF-κB activation when only one *TNFAIP3* allele is lost. Interestingly, tumour cells from patients with *KLHL6* mutations had a higher NF-κB activity, although this signature was not only confined to cases in which *KLHL6* was mutated (Supplementary Fig. 7f).

To investigate whether the tumour suppressor role of *KLHL6* would be diminished in *TNFAIP3*-null ABC-DLBCLs, we ablated *KLHL6* in RCK8 cells[14] and observed no significant effects on cellular proliferation (Fig. 7h) and apoptosis (Fig. 7i). Additionally, utilizing shRNAs targeting roquin2 in both HBL1 (wild-type *TNFAIP3*) and HLY1 (*TNFAIP3*-null[41]) cells, we observed elevated apoptosis only in HBL1 cells (Fig. 7j), indicating the relevance of roquin2 in cells harbouring a functional *TNFAIP3* gene.

Discussion

KLHL6 is a BTB-kelch domain protein mutated in human DLBCL. Somatic mutations localize to the BTB-domain with relevant hotspots at amino acids 65 and 90[4–7]. Most *KLHL6* alterations in DLBCL include monoallelic missense mutations and infrequent copy loss[4–7]. Mutations in *KLHL6* are probably the consequence of aberrant hypersomatic mutation[42], similarly to those in BCL6 and MYC[43]. Importantly, the hotspots and other deleterious BTB-domain mutations result in loss of both cullin3 interaction and E3 ligase activity. Data from VAL cells suggest that mutations might be accompanied by transcriptional downregulation, resulting in a loss of function. Indeed, about 6% of DLBCL tumours showed downregulation of the *KLHL6* transcript. In ABC-DLBCL cell lines, ablation of *KLHL6* promotes cell growth both in vitro and in vivo, supporting a tumour suppressor role. These findings are consistent with low *KLHL6* expression levels correlating with poorer survival in ABC-DLBCL patients[29,30].

Furthermore, we identified roquin2 as the bona fide substrate of KLHL6. KLHL6 specifically binds, ubiquitylates and triggers roquin2 (but not roquin1) degradation in a BCR-dependent manner. Expression of a non-degradable roquin2(Y691F) mutant phenocopies loss of KLHL6 and concomitant ablation of roquin2 in KLHL6$^{-/-}$ cells results in an inhibition of cell proliferation. This pro-proliferative effect depends on the ability of roquin2 to bind RNA[18–22]. Although roquin1 and roquin2 are genetically redundant in the T-cell compartment[21], no studies have assessed the functional redundancy in B-cell cancers. Transgenic mice overexpressing roquin2 or the non-degradable mutant in the germinal centre might be helpful to model the oncogenic role of roquin2 in DLBCL in vivo.

TNFAIP3 is a relevant target of roquin2-mediated mRNA decay[19]. In ABC-DLBCL, BCR-signaling triggers transcription of *KLHL6* and degradation of roquin2, thus releasing *TNFAIP3* from mRNA decay. We speculate that KLHL6-dependent inhibition of *TNFAIP3* decay via roquin2 degradation contributes to establishing a negative feedback loop to terminate the NF-κB signaling (Fig. 7k). Thus, loss of KLHL6 function promotes BCR-dependent activation of NF-κB in ABC-DLBCL. Correspondingly, mutations in *KLHL6* correlate with high NF-κB signatures and could serve as a marker of resistance to NF-κB pathway-targeting drugs such as ibrutinib[13], MLN4924[33] or bortezomib[1].

TNFAIP3 genetic mutations and deletions are frequently observed in ABC-DLBCLs[12–15]. Functional reconstitution of TNFAIP3 in *TNFAIP3*-null DLBCL causes apoptosis and growth arrest, supporting a tumour suppressor role in DLBCL[44,45]. Interestingly, co-occurrence of mutations in the *KLHL6* BTB-domain and biallelic deletion of or mutations in *TNFAIP3* was

rarely observed in human DLBCL, suggesting that these two genes may have similar downstream components (that is, IKK activation). A partial overlap between mutations in the *KLHL6* BTB-domain and monoallelic deletion of *TNFAIP3* further points to a possible synergy towards NF-κB activation. On the other hand, neither roquin2 amplification nor sequence alteration of *TNFAIP3* mRNA at the roquin2-binding site has been observed in DLBCLs. This suggests that the tumour suppressor mechanism of KLHL6 might extend beyond roquin2–*TNFAIP3* deregulation. It is possible that KLHL6 might be involved in other biological processes such as cell adhesion, migration or immune surveillance in patients.

Much remains to be done to evaluate the functional impact of the KLHL6–roquin2 axis in GCB-DLBCLs, in which unknown KLHL6 substrates or different mRNA targets of roquin2 can contribute to the proliferation and survival of GCB-DLBCL cells. It is also worth noting that *KLHL6* mutations are not observed at high frequency in non-B-cell cancers, suggesting a possibly differential role for KLHL6 in a different genetic and cellular context.

Methods

Methods, including statements of data availability and any associated accession codes and references, are available at https://doi.org/10.1038/s41556-018-0084-5.

Received: 1 March 2017; Accepted: 13 March 2018;
Published online: 25 April 2018

References

1. Yang, Y. & Staudt, L. M. Protein ubiquitination in lymphoid malignancies. *Immunol. Rev.* **263**, 240–256 (2015).
2. Gupta-Rossi, N. et al. Specific over-expression of deltex and a new kelch-like protein in human germinal center B cells. *Mol. Immunol.* **39**, 791–799 (2003).
3. Kroll, J. et al. The BTB-kelch protein KLHL6 is involved in B-lymphocyte antigen receptor signaling and germinal center formation. *Mol. Cell Biol.* **25**, 8531–8540 (2005).
4. Morin, R. D. et al. Frequent mutation of histone-modifying genes in non-Hodgkin lymphoma. *Nature* **476**, 298–303 (2011).
5. Lohr, J. G. et al. Discovery and prioritization of somatic mutations in diffuse large B-cell lymphoma (DLBCL) by whole-exome sequencing. *Proc. Natl Acad. Sci. USA* **109**, 3879–3884 (2012).
6. García-Ramírez, I. et al. *Crebbp* loss cooperates with *Bcl2* overexpression to promote lymphoma in mice. *Blood* **129**, 2645–2656 (2017).
7. Reddy, A. et al. Genetic and functional drivers of diffuse large B cell lymphoma. *Cell* **171**, 481–494 (2017).
8. Alizadeh, A. A. et al. Distinct types of diffuse large B-cell lymphoma identified by gene expression profiling. *Nature* **403**, 503–511 (2000).
9. Rosenwald, A. et al. Molecular diagnosis of primary mediastinal B cell lymphoma identifies a clinically favorable subgroup of diffuse large B cell lymphoma related to Hodgkin lymphoma. *J. Exp. Med.* **198**, 851–862 (2003).
10. Staudt, L. M. Oncogenic activation of NF-κB. *Cold Spring Harb. Perspect. Biol.* **2**, a000109 (2010).
11. Young, R. M., Shaffer, A. L. 3rd, Phelan, J. D. & Staudt, L. M. B-cell receptor signaling in diffuse large B-cell lymphoma. *Semin Hematol.* **52**, 77–85 (2015).
12. Lenz, G. et al. Oncogenic CARD11 mutations in human diffuse large B cell lymphoma. *Science* **319**, 1676–1679 (2008).
13. Davis, R. E. et al. Chronic active B-cell-receptor signalling in diffuse large B-cell lymphoma. *Nature* **463**, 88–92 (2010).
14. Compagno, M. et al. Mutations of multiple genes cause deregulation of NF-κB in diffuse large B-cell lymphoma. *Nature* **459**, 717–721 (2009).
15. Kato, M. et al. Frequent inactivation of A20 in B-cell lymphomas. *Nature* **459**, 712–716 (2009).
16. Fu, M. & Blackshear, P. J. RNA-binding proteins in immune regulation: a focus on CCCH zinc finger proteins. *Nat. Rev. Immunol.* **17**, 130–143 (2017).
17. Kataoka, K. et al. Aberrant PD-L1 expression through 3′-UTR disruption in multiple cancers. *Nature* **534**, 402–406 (2016).
18. Leppek, K. et al. Roquin promotes constitutive mRNA decay via a conserved class of stem-loop recognition motifs. *Cell* **153**, 869–881 (2013).
19. Murakawa, Y. et al. RC3H1 post-transcriptionally regulates A20 mRNA and modulates the activity of the IKK/NF-κB pathway. *Nat. Commun.* **6**, 7367 (2015).
20. Glasmacher, E. et al. Roquin binds inducible costimulator mRNA and effectors of mRNA decay to induce microRNA-independent post-transcriptional repression. *Nat. Immunol.* **11**, 725–733 (2010).
21. Vogel, K. U. et al. Roquin paralogs 1 and 2 redundantly repress the Icos and Ox40 costimulator mRNAs and control follicular helper T cell differentiation. *Immunity* **38**, 655–668 (2013).
22. Schlundt, A. et al. Structural basis for RNA recognition in roquin-mediated post-transcriptional gene regulation. *Nat. Struct. Mol. Biol.* **21**, 671–678 (2014).
23. Yu, D. et al. Roquin represses autoimmunity by limiting inducible T-cell co-stimulator messenger RNA. *Nature* **450**, 299–303 (2007).
24. Puente, X. S. et al. Non-coding recurrent mutations in chronic lymphocytic leukaemia. *Nature* **526**, 519–524 (2015).
25. Lohr, J. G. et al. Widespread genetic heterogeneity in multiple myeloma: implications for targeted therapy. *Cancer Cell* **25**, 91–101 (2014).
26. Green, M. R. et al. Transient expression of Bcl6 is sufficient for oncogenic function and induction of mature B-cell lymphoma. *Nat. Commun.* **5**, 3904 (2014).
27. Lydeard, J. R., Schulman, B. A. & Harper, J. W. Building and remodelling Cullin–RING E3 ubiquitin ligases. *EMBO Rep.* **14**, 1050–1061 (2013).
28. Lo, S. C., Li, X. C., Henzl, M. T., Beamer, L. J. & Hannink, M. Structure of the Keap1:Nrf2 interface provides mechanistic insight into Nrf2 signaling. *Embo J.* **25**, 3605–3617 (2006).
29. Meriranta, L. et al. Low expression and somatic mutations of the *KLHL6* gene predict poor survival in patients with activated B-cell like diffuse large B-cell lymphoma. *Blood* **128**, 2926 (2016).
30. Kunder, C. A. et al. KLHL6 is preferentially expressed in germinal center-derived B-cell lymphomas. *Am. J. Clin. Pathol.* **148**, 465–476 (2017).
31. Satpathy, S. et al. Systems-wide analysis of BCR signalosomes and downstream phosphorylation and ubiquitylation. *Mol. Syst. Biol.* **11**, 810 (2015).
32. Lenz, G. et al. Aberrant immunoglobulin class switch recombination and switch translocations in activated B cell-like diffuse large B cell lymphoma. *J. Exp. Med.* **204**, 633–643 (2007).
33. Milhollen, M. A. et al. MLN4924, a NEDD8-activating enzyme inhibitor, is active in diffuse large B-cell lymphoma models: rationale for treatment of NF-κB-dependent lymphoma. *Blood* **116**, 1515–1523 (2010).
34. Zhao, B. et al. The NF-κB genomic landscape in lymphoblastoid B cells. *Cell Rep.* **8**, 1595–1606 (2014).
35. Zhou, A., Scoggin, S., Gaynor, R. B. & Williams, N. S. Identification of NF-B-regulated genes induced by TNFα utilizing expression profiling and RNA interference. *Oncogene* **22**, 2054–2064 (2003).
36. Tian, B., Nowak, D. E., Jamaluddin, M., Wang, S. & Brasier, A. R. Identification of direct genomic targets downstream of the nuclear factor-κB transcription factor mediating tumor necrosis factor signaling. *J. Biol. Chem.* **280**, 17435–17448 (2005).
37. Mansouri, L. et al. Frequent *NFKBIE* deletions are associated with poor outcome in primary mediastinal B-cell lymphoma. *Blood* **128**, 2666–2670 (2016).
38. Boice, M. et al. Loss of the HVEM tumor suppressor in lymphoma and restoration by modified CAR-T cells. *Cell* **167**, 405–418 (2016).
39. Chu, Y. Y. et al. B cells lacking the tumor suppressor TNFAIP3/A20 display impaired differentiation and hyperactivation and cause inflammation and autoimmunity in aged mice. *Blood* **117**, 2227–2236 (2011).
40. Leiserson, M. D. M., Reyna, M. A. & Raphael, B. J. A weighted exact test for mutually exclusive mutations in cancer. *Bioinformatics* **32**, i736–i745 (2016).
41. Fontan, L. et al. MALT1 small molecule inhibitors specifically suppress ABC-DLBCL in vitro and in vivo. *Cancer Cell* **22**, 812–824 (2012).
42. Puente, X. S. et al. Whole-genome sequencing identifies recurrent mutations in chronic lymphocytic leukaemia. *Nature* **475**, 101–105 (2011).
43. Pasqualucci, L. et al. Hypermutation of multiple proto-oncogenes in B-cell diffuse large-cell lymphomas. *Nature* **412**, 341–346 (2001).
44. Honma, K. et al. TNFAIP3/A20 functions as a novel tumor suppressor gene in several subtypes of non-Hodgkin lymphomas. *Blood* **114**, 2467–2475 (2009).
45. Schmitz, R. et al. TNFAIP3 (A20) is a tumor suppressor gene in Hodgkin lymphoma and primary mediastinal B cell lymphoma. *J. Exp. Med.* **206**, 981–989 (2009).
59. Lenz, G. et al. Stromal gene signatures in large-B-cell lymphomas. *N. Engl. J. Med.* **359**, 2313–2323 (2008).

Acknowledgements

We thank C. Vinuesa for providing roquin cDNAs, A. Thomas-Tikhonenko, L. Pasqualucci and Y. Yang for providing DLBCL cell lines, M. Pagano for providing FBP cDNAs, B. Kim for helping with the 3D Matrigel colony formation assay; R. Saffie, D. Brady, E. Witze and R. Greenberg for critically reading the manuscript. This work was supported in part by grant R00-CA166181-04, R01-CA207513-01 from the National Cancer Institute and Gilead Sciences Research Scholars Program in Hematology/Oncology to L.B. R.B. is supported by an NIH Innovator Award (DP2MH107055), the

Searle Scholars Program (15-SSP-102), the March of Dimes Foundation (1-FY-15-344) and the W.W. Smith Charitable Trust (C1404).

Author Contributions

L.B. conceived, directed the project and oversaw the results. J.C. designed and performed most experiments. K.L. helped J.C. with experiments in Figs. 1i,3b,d,4h,6a,7h,j and Supplementary Figs. 3b, 4h. K.I. helped J.C. with experiments in Fig. 6b. R.B. helped with the bioinformatics analysis of RNA-seq data. A.S., L.F. and M.P.W. performed the mass spectrometry analysis of the KLHL6 complex purified by L.B. M.R.G. and S.T. helped with Figs. 1a,b and 3a,7g and Supplementary Figs. 1a,b, 7e,f. L.B. and J.C. wrote the manuscript.

Competing interests

The authors declare no competing interests.

Additional information

Supplementary information is available for this paper at https://doi.org/10.1038/s41556-018-0084-5.

Reprints and permissions information is available at www.nature.com/reprints.

Correspondence and requests for materials should be addressed to L.B.

Publisher's note: Springer Nature remains neutral with regard to jurisdictional claims in published maps and institutional affiliations.

Methods

Cell culture and drug treatment. HEK293T cells were maintained in Dulbecco's modified Eagle's medium (DMEM) containing 10% fetal bovine serum (FBS). U2932, BJAB, SUDHL4, SUDHL6, RAMOS, TMD8, HBL1, Pfeiffer, OCI-LY8, Karpas422, ARP1, RCK8, HLY-1, SUDHL10 and VAL cells were maintained in RPMI 1640 medium containing 10% FBS. OCI-LY1, OCI-LY7, OCI-LY10 and OCI-LY19 cells were maintained in Iscove's modified Dulbecco's Medium (IMDM) containing 10% FBS. For the BCR-crosslinking experiment, Goat-F(ab′)$_2$ anti-human IgM (SouthernBiotech, 2022-01) was used at the indicated concentrations. For the 3D Matrigel colony formation assay, 150 µl of Corning Matrigel Basement Membrane Matrix was used in mix of 100 µl of DMEM/F12 containing 10% knockout serum replacement and plated in Millicell EZ slides (Millipore). For quantification of cell numbers from colonies grown for 14 days, 300 µl of Corning Dispase (354235) was used according to the manufacturers' protocols. The following drugs were used: proteasome inhibitor MG132 (Peptide Institute Inc., 10 µM final concentration), cycloheximide (Sigma-Aldrich, 50 µg ml^{-1} final concentration), MLN4924 (Active Biochem, 5 µM final concentration), IKK-16 (Selleckchem, 10 µM final concentration), ibrutinib (Selleckchem, 5 µM final concentration), actinomycinD (Sigma-Aldrich, 2 µg ml^{-1} final concentration), doxycycline hyclate (Sigma-Aldrich, 1 µg ml^{-1} final concentration). When indicated, cells were selected with puromycin (Sigma-Aldrich, 0.5–1 µg ml^{-1} final concentration) and hygromycin (ThermoFisher, 100 µg ml^{-1}). MTS assays (Promega, G5421) and AnnexinV staining (ThermoFisher AnnexinV, AlexaFluor-680 conjugate; A35109) were performed according to the manufacturers' protocols. For detection of IgM and IgG surface expression, FITC mouse anti-human IgM (BD, 562029) and APC mouse anti-human IgG (BD, 562025) were used according to the manufacturers' instructions.

Biochemical methods. Extract preparation, immunoprecipitation and immunoblotting, fractionation of DLBCLs and chromatin immunoprecipitation were carried out as previously described[46]. Band quantification was performed using ImageJ software and plotted using a nonlinear-fit curve in Graphpad Prism (Graphpad Prism 6). All antibodies were used at a dilution of 1:1,000 unless specified. The following antibodies were used: anti-Flag (Sigma-Aldrich, F7425, 1:3,000), anti-HA (Biolegend, 901513), anti-cullin1 (Invitrogen, 71-8700), anti-cullin3 (Bethyl Laboratories, A301-109A), anti-ubiquitin K48 (EMD Millipore, 05-1307), anti-roquin1/2 (EMD Millipore, MABF288), anti-roquin2 (Santa Cruz, sc-165026), anti-roquin2 (Bethyl Laboratories, A305-150A), anti-KLHL6 (Abcam, ab182163), anti-KLHL6 (Novus Biologicals, NBP1-46128), anti-tubulin (Santa Cruz, sc-8035), anti-GAPDH (EMD Millipore, MAB374, 1:5,000), anti-CDK1 (Santa Cruz, sc-954), anti-CDK2 (Santa Cruz, sc-163), anti-p-AKT S473 (Cell Signaling Technology, 4051), anti-p-ERK T202/Y204 (Cell Signaling Technology, 9101), anti-ERK1/2 (Cell Signaling Technology, 9102), anti-AKT (Cell Signaling Technology, 4691), anti-TNFAIP3 (Cell Signaling Technology, 5630), anti-p-Iκ B S32 (Cell Signaling Technology, 2859, 1:500), anti-p100/p52 (Cell Signaling Technology, 4882), anti-p105/p50 (Santa Cruz, sc-7178), anti-RelA (Santa Cruz, sc-372), anti-RelB (Santa Cruz, sc-226), anti-histone H2A (EMD Millipore, 07-146) and anti-histone H3 (Abcam, ab1791, 1:5,000), ECL rabbit IgG HRP-linked whole antibody (GE Healthcare, NA934-1ML, 1:5,000), ECL mouse IgG, HRP-linked whole antibody (GE Healthcare, NA931-1ML, 1:5,000), anti-rat IgG (H + L) polyclonal antibody (Jackson Immunoresearch, 112-035-003, 1:5,000), anti-goat IgG (H + L) polyclonal antibody (Jackson Immunoresearch, 705-035-003, 1:5,000). KLHL6, roquin1/2, TNFAIP3, cullin1, cullin3, p100/p52, p105/p50 and RelA antibodies were validated in our laboratory utilizing RNA interference as well as overexpression, and were also validated by the manufacturer. All other primary antibodies were validated on the manufacturer's datasheets.

The following agarose beads were used: anti-Flag-M2 affinity gel (Sigma-Aldrich, A2220) and Strep-Tactin Superflow 50% suspension (Neuromics).

Xenotransplantation experiments. All animal work was performed following the ethical guidelines and protocols approved by the Institutional Animal Care and Use Committee of the University of Pennsylvania. NSG mice were purchased from the Jackson Laboratory. Six to eight-week-old NSG mice received subcutaneous flank injections of 1×10^7 U2932 KLHL6$^{-/-}$ (clone-derived) cells that expressed empty vector, KLHL6(WT) or KLHL6(S94I)), and 1×10^7 U2932 cells infected with retroviruses encoding HA–roquin2(WT) or HA–roquin3H2(Y691F) in 100 µl sterile PBS. Tumour burden was monitored weekly by palpation and visual inspection. Tumour volume was calculated by caliper measurement. Tumour weight was analysed on the excised tumours at the experimental endpoint using an analytical scale. After about one month, tumour volume and weight were measured.

Purification and analysis of KLHL6 interactors. Approximately 5×10^8 HEK293T and ARP-1 cells stably expressing Flag-tagged KLHL6(WT) or Flag-tagged KLHL6(L65P) cells were harvested and subsequently lysed in lysis buffer (50 mM Tris-HCl pH 7.5, 150 mM NaCl, 1 mM EDTA, 50 mM NaF, 0.5% NP-40, plus protease and phosphatase inhibitors). KLHL6 was immunopurified with an anti-Flag agarose resin (Sigma-Aldrich) and washed five times with lysis buffer (15 min each). After washing, proteins were eluted with Flag peptides (Sigma-Aldrich). The eluates (1% of the immunoprecipitate) were separated by SDS–PAGE, and proteins were stained by silver staining (Life Technology). The final eluate was then precipitated with trichloroacetic acid.

In vitro ubiquitylation assay. The ubiquitylation of KLHL6 and roquin2 was performed in a volume of 10 µl, containing 50 mM Tris pH 7.6, 5 mM $MgCl_2$, 2 mM ATP, 1.5 ng µl^{-1} E1 (Boston Biochem), 10 ng µl^{-1} UBCH5C, 2.5 µg µl^{-1} ubiquitin (Sigma-Aldrich), 1 µM ubiquitin aldehyde, and purified Flag–KLHL6 or Flag–KLHL6 and HA–roquin2 complex from HEK293T cells obtained by Flag immunoprecipitation. The reactions were incubated at 37 °C for the indicated times, subjected to SDS–PAGE, then analysed by immunoblot. When indicated, upon reaction, beads were resuspended in 1% SDS, boiled, then diluted to 0.1% SDS. The eluted proteins were further Flag-immunoprecipitated, washed and eluted in Laemmli buffer before SDS–PAGE analysis.

In vivo ubiquitylation assay. U2932 *KLHL6*$^{+/+}$ and *KLHL6*$^{-/-}$ (clone-derived) cells were treated with or without MG132 for 6 h and lysed in 1% SDS. Lysates were then diluted to 0.1% SDS in NP-40 buffer and immunoprecipated with a polyclonal antibody against roquin2. The immunocomplexes were subjected to SDS–PAGE and analysed by immunoblot.

In vitro binding assays. For in vitro binding assays, in vitro-translated Flag-tagged KLHL6 was added to lysis buffer (50 mM Tris-HCl pH 7.5, 250 mM NaCl, 0.1% Triton X-100, 1 mM EGTA) with indicated amounts of roquin2 peptides. Anti-streptavidin resin was then added to the lysis buffer and incubated at 4 °C for 2 h. Samples were washed three times with the lysis buffer, and complexes were eluted in Laemmli buffer. For the use of HEK293T cells stably expressing KLHL6(WT), cells were lysed with the lysis buffer and anti-streptavidin resin was directly added to the whole-cell lysates with the peptides.

Transient transfections and retrovirus-mediated gene transfer. HEK293T cells were transfected using polyethylenimine. For retrovirus and lenvirius production, GP-293 packaging cells (Clontech) or pCMV-DeltaR8.2 were used respectively. The virus-containing medium was collected after 48 h of transfection and supplemented with 10 µg ml^{-1} polybrene (Sigma-Aldrich). Then, cells were spin-infected at 1,800 r.p.m. for 30 min with the viral supernatant for 6 h to overnight. For RCK8, cells were electroporated using Neon transfection system according to manufacturer's protocol with LentiCRISPRv2 vector carrying a GFP marker. Transfected cells were sorted by GFP. siRNA oligos transfection was performed with Neon transfection system.

Generating clonal KLHL6$^{-/-}$ cell lines. U2932 or OCI-LY10 Cas9-expressing cells were infected with lentiviruses encoding gRNAs targeting the *KLHL6* exon1. Upon infection and puromycin selection, cells were plated in a 96-well plate at a concentration of 0.5 cells per well. Single clones were screened for KLHL6 expression by immunoblotting.

Plasmids. Human roquin1 and roquin2 cDNA were provided by C. Vinuesa and subcloned into pcDNA3.1-Flag, pcDNA3.1-HA or pcDNA3.1-Flag-streptavidin. Human *KLHL6* cDNA was purchased from Dharmacon and subcloned into pcDNA3.1-Flag, pcDNA3.1-Flag-streptavidin, pREV-TRE. C-terminal deletion mutants and point mutants were generated by utilizing the QuikChange Site-directed Mutagenesis kit (Stratagene), and N-terminal deletion mutants were generated by standard PCR methods. For retrovirus production, cDNAs encoding Flag-tagged or HA-tagged KLHL6 and KLHL6 mutants were subcloned into the retroviral vector MIGR1 and pREV-TRE vector. cDNAs encoding Flag–HA-tagged or untagged roquin2 and roquin2 mutants were subcloned into the retroviral vector pBabe Puro or pMSCV. Lentivirus encoding shRNAs targeting human KLHL6 were subcloned in pSicoR-Puro. Lentivirus encoding shRNAs targeting human roquin2 were subcloned in pSicoR-GFP.

KLHL6 cDNA was clone into pTRIPZ using AgeI and HpaI.

The target sequences used to knockdown human *KLHL6* were:

h*KLHL6* shRNA1:
forward: TGCAGCCAGCAACTATTTCATTCAAGAGATGAAATAG-TTGCTGGCTGCTTTTTTC,
reverse: TCGAGAAAAAAGCAGCCAGCAACTATTTCATCTCTTGAA-TGAAATAGTTGCTGGCTGCA;

h*KLHL6* shRNA2:
forward: TGAAGCCTTGAACCCAGAAATTCAAGAGATTTCTGGG-TTCAAGGCTTCTTTTTTC,
reverse: TCGAGAAAAAAGAAGCCTTGAACCCAGAAATCTCTTGAA-TTTCTGGGTTCAAGGCTTCA;

h*KLHL6* shRNA3:
forward: TGCATGATGTTTGGAAATAT
TTCAAGAGAATATTTCCAAACATCATGCTTTTTTC,
reverse: TCGAGAAAAAA GCATGATGTTTGGAAATAT
TCTCTTGAAATATTTCCAAACATCATGCA;

h*KLHL6* shRNA4:
forward: TGGATTCAGATTGAGTATTT
TTCAAGAGAAAATACTCAATCTGAATCCTTTTTTC,

reverse: TCGAGAAAAAA GGATTCAGATTGAGTATTT TCTCTTGAAAAATACTCAATCTGAATCCA.
The target sequences used to knockdown human roquin2 were:
hroquin2 shRNA1:
forward: TGCAGTTGTCTGCCAATCTATTCAAGAGATAGATTGG-CAGACAACTGCTTTTTTC,
reverse:TCGAGAAAAAAGCAGTTGTCTGCCAATCTATCTCTTG-AATAGATTGGCAGACAACTGCA;
hroquin2 shRNA2:
forward: TGGACTCAGATACCCTTTGATTCAAGAGATCAAAGGG-TATCTGAGTCCTTTTTTC,
reverse:TCGAGAAAAAAGGACTCAGATACCCTTTGATCTCTTGAATCAA AGGGTATCTGAGTCCA.
Lentiviruses encoding gRNAs targeting human *KLHL6* were subcloned into a Lenti-Guide-Puro vector, Lenti-Guide-GFP and LentiCRISPRv2 vector.
The target sequences to knockout human *KLHL6* were:
h*KLHL6* gRNA2: forward: CAGAGCGTTTTCCATTCGCA,
reverse: TGCGAATGGAAAACGCTCTG;
h*KLHL6* gRNA3: forward: TCAGAGCGTTTTCCATTCGC,
reverse: GCGAATGGAAAACGCTCTGA;
h*KLHL6* gRNA4 forward: AAAGGTCAAATTTGACGACG,
reverse: CGTCGTCAAATTTGACCTTT;
h*KLHL6* gRNA5: forward: GACTTGGTCGAGATCTTAAA,
reverse: TTTAAGATCTCGACCAAGTC;
h*KLHL6* gRNA6: forward: ACTTGGTCGAGATCTTAAAT,
reverse: ATTTAAGATCTCGACCAAGT.

Gene silencing by siRNA. For siRNA-mediated silencing, duplexes were purchased from Dharmacon. The target sequence for human *KLHL6* siRNA was GCACGAAGGAUGAACGGUU. The target sequence for human roquin2 siRNA was GCUUGAAAAGUAUCGAUUA. Non-targeting siRNA control sequence was UGGUUUACAUGUCGACUAA.

mRNA analysis. RNA was extracted using the RNeasy Kit (Qiagen) and TRIzol (Invitrogen). cDNA synthesis was performed using the Maxima First-Strand cDNA Synthesis kit (ThermoFisher) and RNA to cDNA Ecodry Premix kit (Clontech). Quantitative PCR analysis using SYBRGreen PCR Master Mix (Applied Biosystems) was performed according to standard procedures. Primer sequences were:
h*GAPDH*: forward: 5′-GGAGCGAGATCCCTCCAAAAT-3′,
reverse: 5′-GGCTGTTGTCATACTTCTCATGG-3′;
h*TNFAIP3*: forward: 5′-TCCTCAGGCTTTGTATTTGAGC-3′,
reverse: 5′-TGTGTATCGGTGCATGGTTTTA-3′;
h*TNFRSF14*: forward: 5′-CCACTGGGTATGGTGGTTTC-3′,
reverse: 5′-TCACCTTCTGCCTCCTGTCT-3′;
h*TNF*: forward: 5′-CTGCACTTTGGAGTGATCGGC-3′,
reverse: 5′-CACCAGCTGGTTATCTCTCAGCTCC-3′;
h*NFKBIE*: forward: 5′-TCTGGCATTGAGTCTCTGCG-3′,
reverse: 5′-AGGAGCCATAGGTGGAATCAG-3′;
h*LTA*: forward: 5′-GCTGCTGGTTCTGCTGCC-3′,
reverse: 5′-CAAGGAGAAACCATCCTGGAGGAAG-3′;
h*NEDD4L* forward: 5′-ACTTCCTCCTCCTCCTGC-3′,
reverse: 5′-TCCAAGTCTTCGCTGATGTG-3′;
h*ABLIM1*: forward: 5′-ACTGCATCTCTCCCTGGCTA-3′,
reverse: 5′-TGTTGGTCACCATGAGCATT-3′;
h*SYNGAP1*: forward: 5′-TCTGAGGAAAACTGCGAGGT-3′,
reverse: 5′-GCAAACACCTCCTTCAGCTC-3′;
h*NEIL2*: forward: 5′-GCCTCCACAAAAAGAAGTGC-3′,
reverse: 5′-TTGTTGGCTTTCTTGGCTCT-3′;
h*LGALS8*: forward: 5′-CTGGGCATTTATGGCAAAGT-3′,
reverse: 5′-GACAGTTCTGGGTGCGATTT-3′;
h*CD274*: forward: 5′-TATGGTGGTGCCGACTACAA-3′,
reverse: 5′-TGCTTGTCCAGATGACTTCG-3′;
h*KLHL6*: forward: 5′-GCAGCCAGCAACTATTTCAGG-3′,
reverse: 5′-ACGTGTAGTCCAACAGAGTGT-3′;
h*NFKBIA*: forward: 5′-TATAAACGCTGGCTGGG-3′,
reverse: 5′-CCCTAGTGGCTCATCGC-3′.

Normalization and quantification of protein levels. Protein concentrations of cell extracts were measured using a Bio-Rad DC protein assay (Lowry assay) according to the manufacturer's protocol. For each experiment, equal amounts of protein (~15 µg) were separated by SDS–PAGE and analysed by immunoblotting. Equal protein levels in each lane were confirmed by PonceauS staining of the membrane and by immunoblotting a constitutively expressed protein.

Cell proliferation assay. 2×10^3 cells were plated for the MTS assay according to the manufacturers' protocols. For the long-term cell proliferation assay, 5×10^4–2×10^5 cells were plated, counted and re-plated every 3–5 days.

Flow cytometry. Flow cytometry was performed on Attune NxT Flow Cytometer using FITC for GFP-expressing cells, Alexa-680 AnnexinV to detect apoptosis, FITC to detect IgM or APC to detect IgG staining. All stainings were performed according to manufacturers' protocols. For investigating shRNA or gRNA effects on survival, 5×10^5 cells were spin-infected in a 24-well plate with 1,000 µl lentivirus-containing medium in the presence of polybrene (8 µg ml^{-1}). Medium was changed after the spin-infection and the number of infected cells was determined on day 2 when GFP was fully expressed in all infected cells. The number of viable GFP$^+$ cells on day 2 was set to 100% to normalize for transduction efficiency and every consecutive assessment was calculated in relation to day 2. When indicated, AnnexinV$^+$ cells were gated on GFP$^+$ cells (see gating strategy in Supplementary Figs. 3, 5).

MudPIT analysis. Trichloroacetic acid-precipitated proteins were urea-denatured, reduced, alkylated and digested with endoproteinase Lys-C (Roche), followed by modified trypsin (Roche), as described[47,48]. Peptide mixtures were loaded onto 100-µm fused silica microcapillary columns packed with 5-µm C18 reverse phase (Aqua, Phenomenex), strong cation exchange particles (Luna, Phenomenex), and reverse phase[49]. Loaded microcapillary columns were placed in-line with a Quaternary Agilent 1100 series HPLC pump and a LTQ linear ion trap mass spectrometer equipped with a nano-liquid chomatography electrospray ionization source (Thermo Scientific). Fully automated 10-step MudPIT runs were carried out on the electrosprayed peptides, as described[47]. Tandem mass spectometry spectra were interpreted using SEQUEST[50] against a database of 61,318 sequences, consisting of 30,449 non-redundant human proteins (downloaded from NCBI on 27 August 2012, 160 usual contaminants (such as human keratins, IgGs and proteolytic enzymes), and, to estimate false discovery rates, 30,659 randomized amino acid sequences derived from each non-redundant protein entry. Peptide/spectrum matches were sorted and selected using DTASelect with the following criteria set: spectra/peptide matches were only retained if they had a DeltCn of at least 0.08 and a minimum XCorr of 1.8 for single-, 2.0 for double-, and 3.0 for triple-charged spectra. In addition, peptides had to be fully tryptic and at least seven amino acids long. Combining all runs, proteins had to be detected by at least two such peptides, or one peptide with two independent spectra. Under these criteria the final false discovery rates (FDRs) at the protein and spectral levels were 2.1% ± 0.3 and 0.94% ± 0.03, respectively. Peptide hits from multiple runs were compared using CONTRAST[51]. To estimate relative protein levels, normalized spectral abundance factors were calculated for each detected protein, as described[52–54].

Analysis of KLHL6 expression in DLBCL patients. Raw DNA copy number data from high-resolution SNP microarray analysis of 609 primary DLBCL tumours were obtained from a previously published study[26]. The data were visualized using the integrative genomics viewer (IGV)[55]. Cases were sorted according to their *KLHL6* copy number status, and those with copy number <1.8 were classified as possessing a deletion, according to previously described criteria[56].

Gene expression microarray from 249 tumours with matched DNA copy number data were obtained from a previously published study[26]. Their cell of origin subtype was determined using the Wright algorithm[57], as previously reported[56]. Row normalized heat maps for four probe sets corresponding to KLHL6 were sorted according to their average expression, and significant reduction in KLHL6 expression defined as being 1 standard deviation below the mean.

Raw CEL files for publicly available Affymetrix U133 plus 2.0 gene expression microarray data for diffuse large B-cell lymphoma tumours (GSE10846, GSE34171, GSE31312) were obtained from the Gene Expression Omnibus. Data were RMA normalized using the ExpressionFileCreator module of GenePattern[58]. Scores to categorize diffuse large B-cell lymphoma tumours by cell of origin subtype were calculated according to the Wright algorithm[57]. Intensities from the 4 probes for KLHL6 (1555275_a_at, 1560396_at, 1560397_s_at, 2281f67_at) were averaged for use in the survival analysis. Cases were dichotomized into being above or below the median expression level of KLHL6 expression within each dataset to avoid confounding batch effects. For NF-κB signatures, Affymetrix U133 plus 2 gene expression microarrays were performed on 84 matched DLBCL tumours[26,59]. Raw CEL files were robust multi-array average (RMA) normalized with median scaling using the ExpressionFileCreator module of GenePattern[58]. Sample-level enrichment of NF-κB target genes was calculated using the single sample gene set enrichment analysis[60] and the c3 TFT gene set database of mSigDB[61].

RNA-seq. Total RNA was extracted from U2932 cells using RNeasy Mini Kit (Qiagen, 74104) and polyA + transcripts isolated with oligo $(dT)_{25}$-conjugated magnetic Dynabeads (ThermoFisher). Strand-specific RNA-seq libraries were prepared following a published protocol[62]. In brief, RNA was chemically fragmented in first strand buffer, converted to cDNA using SuperScript III reverse transcriptase (Invitrogen), end-repaired, A-tailed and ligated to custom-designed universal adapters using an end-repair mix, klenow fragment and T4 DNA ligase (all from Enzymatics). After ligation, adapters were removed by SPRI purification using SPRIselect beads (Beckman Coulter) and amplified with Q5 Hot Start DNA polymerase (New England Biolabs) while introducing custom dual indexes. Three biological replicates were sequenced on a NextSeq 500 (Illumina)

at a depth of at least 2×10^7 reads each. Reads were mapped and analysed with a custom bioinformatic pipeline based on STAR[63], SAMTOOLS[64] and the R packages DEGseq[65] and DEseq2[66]. We used human genome version GRCh38 and gene annotations from the ENSEMBL release 83. Gene Ontology analyses were performed using version 6.8 of the DAVID web server[67,68].

ChIP–seq. The data discussed in this publication were obtained from the NCBI's Gene Expression Omnibus[34] and are accessible through GEO with series accession number GSE55105. FASTQs were downloaded and mapped to hg19 with Bowtie2 (v.2.1.0). Genome browser tracks were generated using custom scripts. When available, biological replicate were merged by taking the mean of the reads density at each position. The data were visualized using IGV[55].

Statistics and reproducibility. All graphs show mean values with error bars signifying the standard deviation (s.d.) as indicated in the figure legends. Exact *P* values for each experiment are provided in Supplementary Table 6. Unless otherwise noted, all immunoblots were successfully repeated at least three times. A one-tailed Student's *t*-test was performed for Fig. 3e (right panel) and a two-tailed Student's *t*-test was used in Fig. 4g. Other analyses performed were one-way ANOVA (Figs. 3c,e (left panel), 5e,6a,7i,j and Supplementary Fig. 3b,f) or two-way ANOVA (Figs. 1i,5b,d,3g,h,6e,7h and Supplementary Figs. 2d, 3d, 4e,h, 5b) as indicated in the figure legends. DEseq2 was performed for RNA-seq analysis in Fig. 6b and Supplementary Table 3. Weighted exclusivity test was performed for Supplementary Table 5. A Mantel–Cox test was performed for survival analysis in Fig. 3a. Pearson's correlation coefficient was used in Supplementary Fig. 2c.

Reporting Summary. Further information on experimental design is available in the Nature Research Reporting Summary linked to this article.

Data availability. RNA–seq data that support the findings of this study have been deposited in the Gene Expression Omnibus (GEO) under accession code GSE93675. Previously published ChIP–seq data were obtained from GEO under accession code GSE55105. *KLHL6* copy number change and expression were calculated through re-analysis of SNP data and microarray from GSE11318, GSE12906, GSE15127, GSE22082, GSE34171 and GSE11318, GSE34171, respectively. Microarray data for DLBCL survival were obtained from GEO accession codes GSE10846, GSE34171, GSE31312. Data for NF-κB signature correlation were retrieved from GSE10846. Raw mass spectrometry data are available from PRIDE (https://www.ebi.ac.uk/pride/archive/) under accession code PXD008963.

Raw data from independent experiments with $n < 5$ can be found in the statistical source data (Supplementary Table 6). Unprocessed immunoblots are provided in Supplementary Fig. 8. All other data supporting the findings of this study are available from the corresponding author on reasonable request.

References

46. Busino, L. et al. Fbxw7α- and GSK3-mediated degradation of p100 is a pro-survival mechanism in multiple myeloma. *Nat. Cell Biol.* **14**, 375–385 (2012).
47. Florens, L. & Washburn, M. P. Proteomic analysis by multidimensional protein identification technology. *Methods Mol. Biol.* **328**, 159–175 (2006).
48. Washburn, M. P., Wolters, D. & Yates, J. R. III. Large-scale analysis of the yeast proteome by multidimensional protein identification technology. *Nat. Biotechnol.* **19**, 242–247 (2001).
49. McDonald, W. H., Ohi, R., Miyamoto, D. T., Mitchison, T. J. & Yates, J. R. III. Comparison of three directly coupled HPLC MS/MS strategies for identification of proteins from complex mixtures: single-dimension LC-MS/MS, 2-phase MudPIT, and 3-phase MudPIT. *Int. J. Mass Spectrom.* **219**, 245–251 (2002).
50. Eng, J. K., McCormack, A. L. & Yates, J. R. III. An approach to correlate tandem mass spectral data of peptides with amino acid sequences in a protein database. *J. Am. Soc. Mass Spectrom.* **5**, 976–989 (1994).
51. Tabb, D. L., McDonald, W. H. & Yates, J. R.III. DTASelect and Contrast: tools for assembling and comparing protein identifications from shotgun proteomics. *J. Proteome Res.* **1**, 21–26 (2002).
52. Florens, L. et al. Analyzing chromatin remodeling complexes using shotgun proteomics and normalized spectral abundance factors. *Methods* **40**, 303–311 (2006).
53. Paoletti, A. C. et al. Quantitative proteomic analysis of distinct mammalian Mediator complexes using normalized spectral abundance factors. *Proc. Natl Acad. Sci. USA* **103**, 18928–18933 (2006).
54. Zybailov, B. et al. Statistical analysis of membrane proteome expression changes in *Saccharomyces cerevisiae*. *J. Proteome Res.* **5**, 2339–2347 (2006).
55. Robinson, J. T. et al. Integrative genomics viewer. *Nat. Biotechnol.* **29**, 24–26 (2011).
56. Monti, S. et al. Integrative analysis reveals an outcome-associated and targetable pattern of p53 and cell cycle deregulation in diffuse large B cell lymphoma. *Cancer Cell* **22**, 359–372 (2012).
57. Wright, G. et al. A gene expression-based method to diagnose clinically distinct subgroups of diffuse large B cell lymphoma. *Proc. Natl Acad. Sci. USA* **100**, 9991–9996 (2003).
58. Reich, M. et al. GenePattern 2.0. *Nat. Genet.* **38**, 500–501 (2006).
60. Barbie, D. A. et al. Systematic RNA interference reveals that oncogenic *KRAS*-driven cancers require TBK1. *Nature* **462**, 108–122 (2009).
61. Liberzon, A. et al. Molecular signatures database (MSigDB) 3.0. *Bioinformatics* **27**, 1739–1740 (2011).
62. Parkhomchuk, D. et al. Transcriptome analysis by strand-specific sequencing of complementary DNA. *Nucleic Acids Res.* **37**, e123 (2009).
63. Dobin, A. et al. STAR: ultrafast universal RNA-seq aligner. *Bioinformatics* **29**, 15–21 (2013).
64. Li, H. et al. The Sequence Alignment/Map format and SAMtools. *Bioinformatics* **25**, 2078–2079 (2009).
65. Wang, L., Feng, Z., Wang, X., Wang, X. & Zhang, X. DEGseq: an R package for identifying differentially expressed genes from RNA-seq data. *Bioinformatics* **26**, 136–138 (2010).
66. Love, M. I., Huber, W. & Anders, S. Moderated estimation of fold change and dispersion for RNA-seq data with DESeq2. *Genome Biol.* **15**, 550 (2014).
67. Huang, D. W., Sherman, B. T. & Lempicki, R. A. Systematic and integrative analysis of large gene lists using DAVID bioinformatics resources. *Nat. Protoc.* **4**, 44–57 (2009).
68. Huang, D. W., Sherman, B. T. & Lempicki, R. A. Bioinformatics enrichment tools: paths toward the comprehensive functional analysis of large gene lists. *Nucleic Acids Res.* **37**, 1–13 (2009).

nature cell biology

SUPPLEMENTARY INFORMATION

https://doi.org/10.1038/s41556-018-0084-5

In the format provided by the authors and unedited.

Loss of KLHL6 promotes diffuse large B-cell lymphoma growth and survival by stabilizing the mRNA decay factor roquin2

Jaewoo Choi[1,2], Kyutae Lee[1,2], Kristin Ingvarsdottir[3], Roberto Bonasio[3], Anita Saraf[4], Laurence Florens[4], Michael P. Washburn[4,5], Saber Tadros[6], Michael R. Green[6,7] and Luca Busino[1,2]*

[1]Department of Cancer Biology, University of Pennsylvania, Philadelphia, PA, USA. [2]Abramson Family Cancer Research Institute, Perelman School of Medicine, University of Pennsylvania, Philadelphia, PA, USA. [3]Epigenetics Institute, Department of Cell and Developmental Biology, University of Pennsylvania, Philadelphia, PA, USA. [4]The Stowers Institute of Medical Research, Kansas City, MO, USA. [5]Department of Pathology and Laboratory Medicine, The University of Kansas Medical Center, Kansas City, KS, USA. [6]Department of Lymphoma and Myeloma, University of Texas MD Anderson Cancer Center, Houston, TX, USA. [7]Department of Genomic Medicine, University of Texas MD Anderson Cancer Center, Houston, TX, USA.
*e-mail: businol@upenn.edu

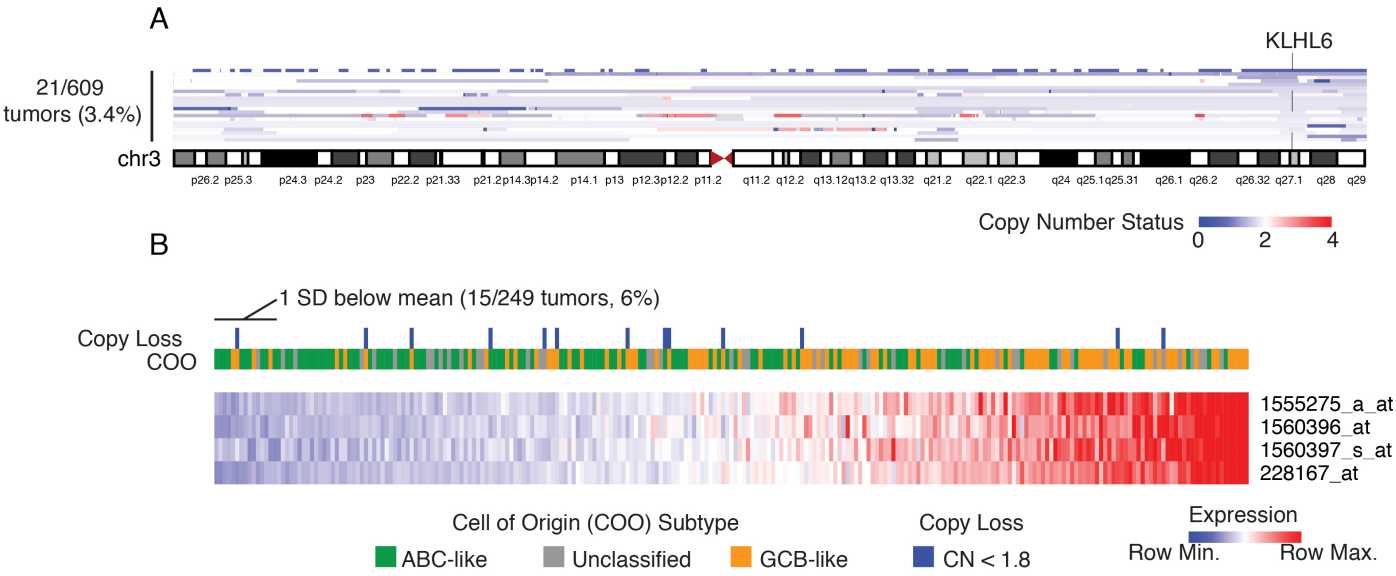

Supplementary Figure 1

Copy number and transcriptional analysis of *KLHL6* in primary DLBCLs.

(a) The DNA copy number of chromosome 3 is shown. DNA copy number data from high-resolution single nucleotide polymorphism (SNP) microarray analysis of 609 primary DLBCL tumors were utilized form a previously published study[26]. The position of *KLHL6* is annotated for 21 DLBCL tumors with copy number <1.8. *KLHL6* loss is detectable in 3.4% of patients. **(b)** A row-normalized heatmap is shown for probe sets corresponding to *KLHL6*. Gene expression microarray from 249 tumors with matched DNA copy number data were obtained from a previously published study[26]. The data are annotated for the cell of origin subtype and DNA copy loss of *KLHL6* as shown in *(a)*. 6% of DLBCL cases with expression ≤1 standard deviation below the mean are indicated.

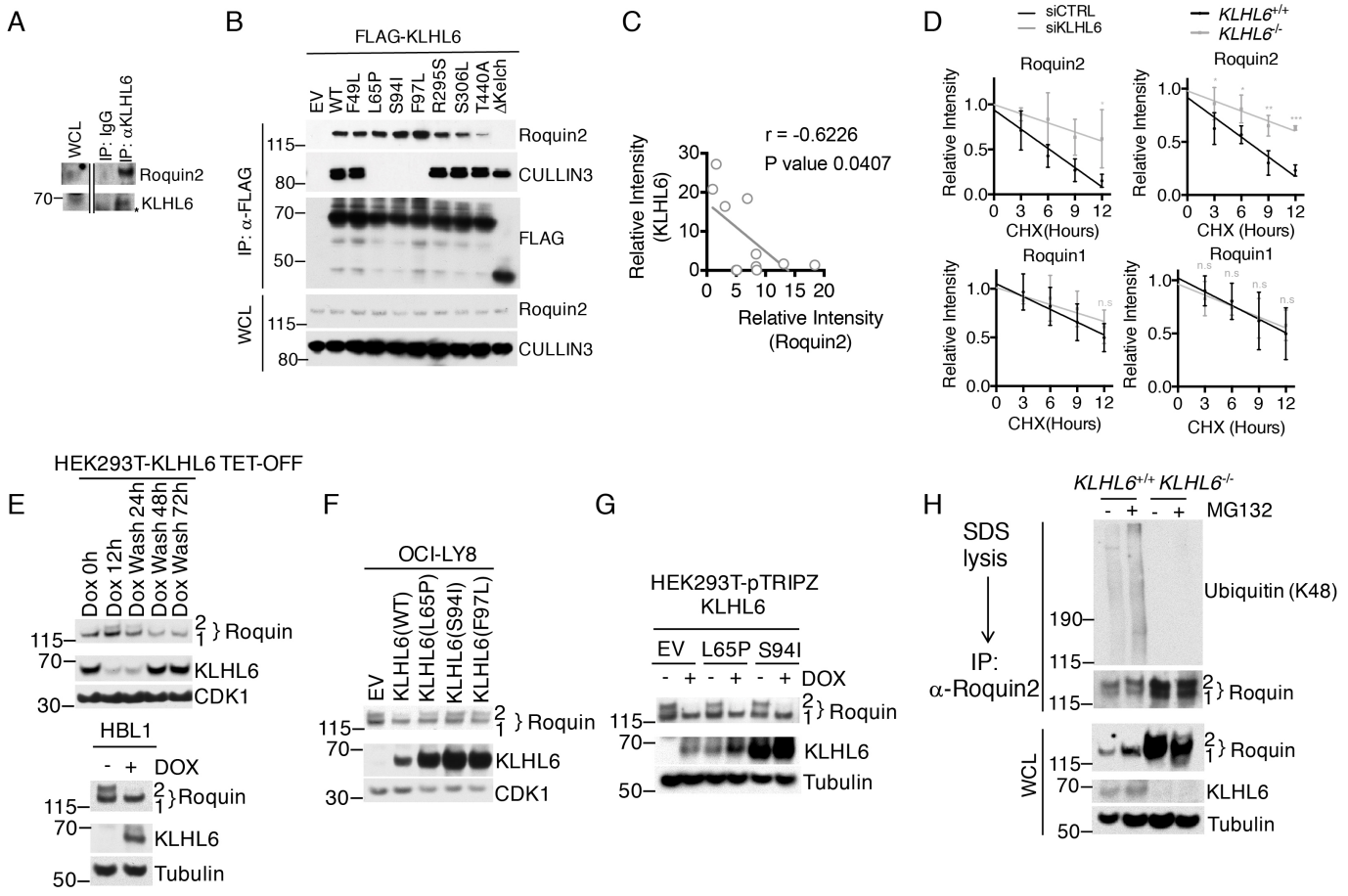

Supplementary Figure 2

KLHL6 WT, but not KLHL6 BTB-mutant, promotes Roquin2 ubiquitylation and degradation.

(a) Immunoblot analysis from immunoprecipitated endogenous KLHL6 in U2932 cells. IgG antibody immunoprecipitates=negative control. A representative blot from two independent experiments is shown. * Non-specific band. **(b)** Immunoblot analysis from immunoprecipitated FLAG-KLHL6 wild type (WT) and mutants in HEK293T cells. EV, empty vector. **(c)** Quantification of Roquin2 (x-axis) and KLHL6 (y-axis) protein levels in each DLBCL cell line. n=11 DLBCL cell lines. r, Pearson correlation coefficient (95% confidence interval). **(d)** Quantification of Roquin1 and Roquin2 immunoblots. Relative intensities were plotted over time for OCI-LY10 (left panel) and U2932 (right panel) (mean±s.d., n=3 independent experiments, two-way ANOVA, *P value≤0.05; **P value≤0.01; *** P value≤0.001; n.s., not significant). **(e)** Immunoblot analysis of whole cell lysates from HEK293T (TET)-OFF cells transduced with retroviruses encoding a doxycycline (DOX) inducible expression of FLAG-tagged KLHL6 carrying a hygromycin cassette (Top panel). DOX was added and/or washed at the indicated times. Bottom panel shows the immunoblot analysis of the indicated proteins in HBL1 cells transduced with lentiviruses encoding a doxycycline (DOX) inducible expression of KLHL6 wild-type (WT) carrying a puromycin cassette. The cells were treated with DOX for 12 hours. **(f)** Immunoblot analysis of whole cell lysates from OCI-LY8 cells transduced with retroviruses encoding empty vector (EV), KLHL6 wild-type (WT) or BTB-mutants (L65P, S94I and F97L) carrying a puromycin cassette. **(g)** Immunoblot analysis of whole cell lysates from HEK293T cells transduced with lentiviruses encoding a doxycline(DOX) inducible expression of KLHL6 carrying a puromycin cassette and infected with lentiviruses encoding empty vector(EV) or KLHL6 BTB-mutants (L65P and S94I) carrying a GFP marker. The cells were treated with DOX for 12 hours. **(h)** Immunoblot analysis of immunoprecipitated endogenous Roquin2 in U2932 *KLHL6*$^{+/+}$ and *KLHL6*$^{-/-}$ (clone-derived) cells treated with or without MG132 for 6 hours. A representative blot from two independent experiments is shown. Unprocessed original scan of immunoblots for *(a,b,e,f,g,h)* are shown in Supplementary Fig. 8, and statistical source data for *(c,d)* and exact P values for *(d)* can be found in Supplementary Table 6. Unless otherwise noted, immunoblots are representative of three independent experiments.

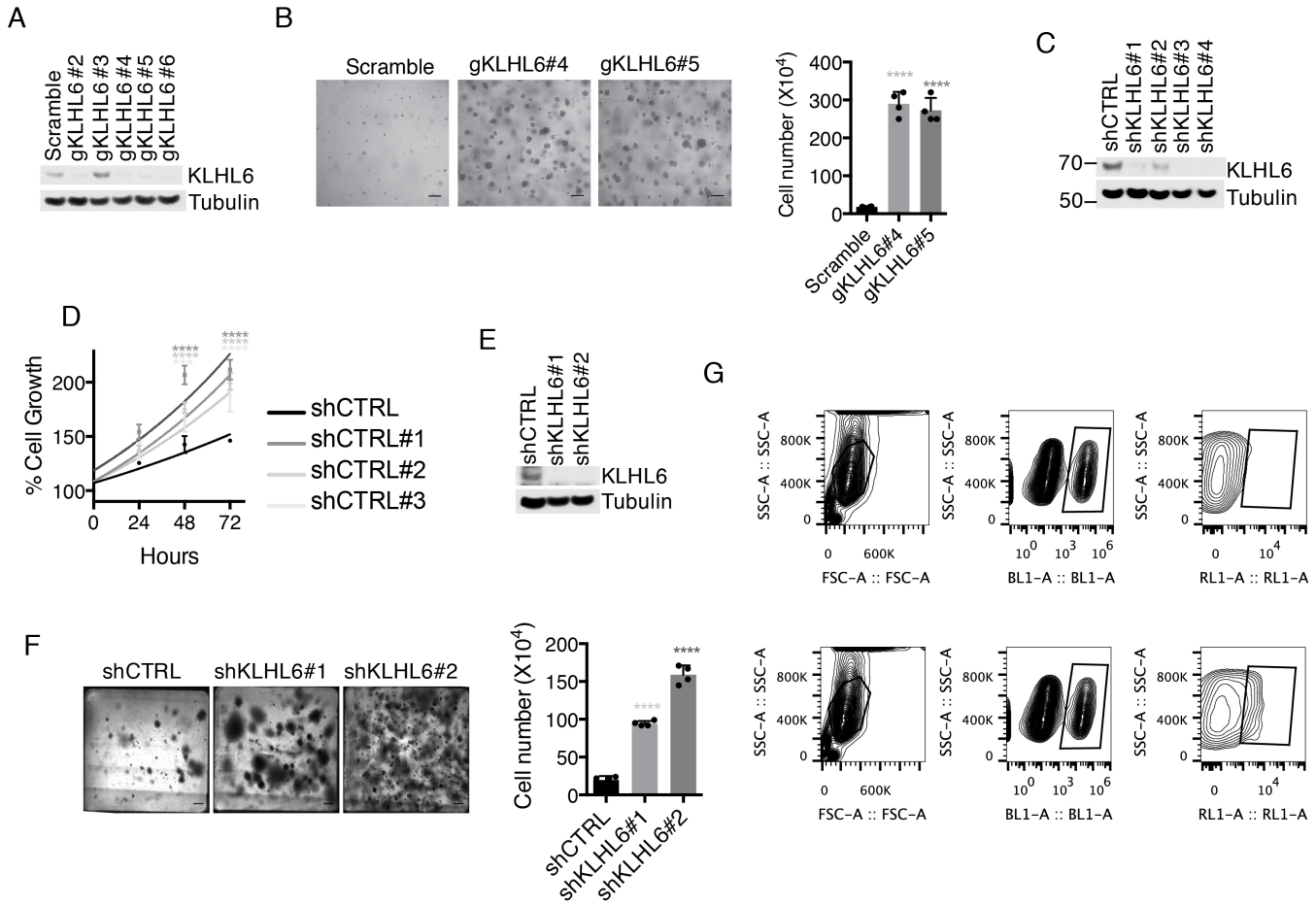

Supplementary Figure 3

Loss of KLHL6 promotes proliferation of ABC-DLBCL cells.

(a) Immunoblot analysis of whole cell lysates from U2932-Cas9 cells infected with lentiviruses encoding scrambled gRNA or gRNAs against KLHL6 exon 1 carrying a puromycin cassette. **(b)** Left panel shows a representative image of U2932 cell colonies expressing indicated gRNAs and plated into a matrigel. After 14 days, the matrigel was dissolved and recovered. Cells were counted and plotted as shown on the right panel (mean±s.d., n=4 independent experiments, one-way ANOVA, ****P value≤0.0001). Scale bar 150μm. **(c)** Immunoblot analysis of whole cell lysates from U2932 cells infected with lentiviruses encoding the indicated shRNAs carrying a puromycin cassette. **(d)** MTS assay for U2932 cells infected with lentiviruses encoding the indicated shRNAs and grown in media containing 1μg/ml of $F(ab')_2$-IgM. Values were normalized to the shCTRL cells at time 0 hour and set as 100% (mean±s.d., n=3 independent experiments, two-way ANOVA; *** P value≤0.001, ****P value≤0.0001). **(e)** Immunoblot analysis of whole cell lysates from OCI-LY10 cells infected with lentiviruses encoding indicated shRNAs carrying a puromycin cassette. **(f)** Left panel shows a representative image of OCI-LY10 cell colonies infected with indicated shRNAs and plated into a matrigel. After 14 days, the matrigel was dissolved and recovered. Cells were counted and plotted as shown on the right panel (mean±s.d., n=4 independent experiments, one-way ANOVA, ****P value ≤0.0001). Scale bar 150μm. **(g)** Gating strategy for Fig. 3c. The box indicates the stained cells. Unprocessed original scan of immunoblots for *(a,c,e)* are shown in Supplementary Fig. 8, and statistical source data and exact P values for *(b,d,f)* can be found in Supplementary Table 6. Unless otherwise noted, immunoblots are representative of three independent experiments.

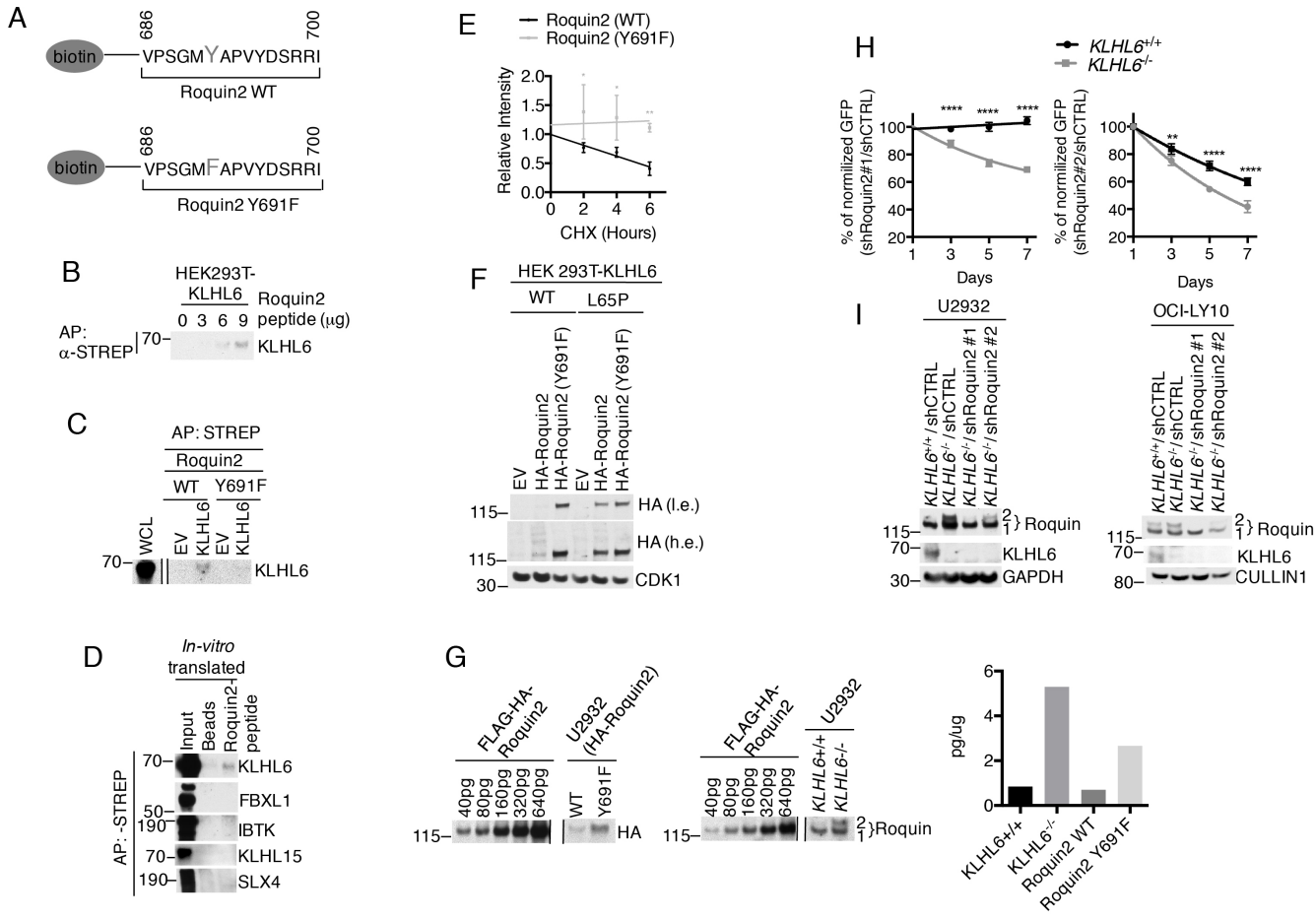

Supplementary Figure 4

The Roquin2(Y691F) mutant is resistant to KLHL6-mediated degradation.

(a) Schematic representation of the sequence of the biotinylated Roquin2 peptides. **(b)** A pull-down assay using the indicated amount of biotinylated Roquin2 peptides incubated with cell extracts from HEK293T cells stably expressing KLHL6. Affinity Purification, AP. **(c and d)** Same as in *(b)* except that FLAG-tagged *in-vitro* translated proteins as indicated were used instead of cell extracts. Immunoblot analysis for the indicated proteins was performed using FLAG antibody. **(e)** Quantification of immunoblots from BJAB cells stably expressing Roquin2(WT) or Roquin2(Y691F). Relative intensities were plotted over time under cycloheximide (CHX) treatment (mean ± s.d., n=3 independent experiments, two-way ANOVA, *P value≤0.05; **P value≤0.01). **(f)** Immunoblot analysis of whole cell lysates from HEK2932T cells stably expressing KLHL6(WT) or KLHL6(L65P) carrying hygromycin cassette and further infected with retroviruses encoding an empty vector(EV), Roquin2(WT) or Roquin2(Y691F) carrying a puromycin cassette. A low exposure (l.e) and high exposure (h.e) are shown. **(g)** Immunoblot analysis for indicated amounts of recombinant Roquin2 (set as the standard) along with whole cell lysates from U2932 stably expressing HA-Roquin2(WT) and HA-Roquin2(Y691F) (left panel) or U2932 *KLHL6*$^{+/+}$ and *KLHL6*$^{-/-}$ cells (clone-derived) (middle panel). Right panel shows intensity of quantified Roquin2 bands compared to the standard. A representative blot from one experiment is shown. **(h)** Flow cytometry analysis of GFP^{+}-live OCI-LY10 *KLHL6*$^{+/+}$ and *KLHL6*$^{-/-}$(clone-derived) cells infected with lentiviruses encoding the indicated shRNAs carrying a GFP marker. Cells were grown in media containing 2μg/ml of F(ab')$_2$-IgM and normalized to the shCTRL cells set as 100% (mean±s.d., n=3 independent experiments, two-way ANOVA, **P value≤0.01; ****P value≤0.0001). **(i)** Immunoblot analysis of whole cell lysates from GFP-sorted U2932 (left panel) and OCI-LY10 (right panel) *KLHL6*$^{+/+}$ and *KLHL6*$^{-/-}$ (clone-derived) infected with lentiviruses encoding the indicated shRNAs carrying a GFP marker. A representative blot from two independent experiments is shown. Unprocessed original scan of immunoblots for *(b,c,d,f,g,i)* are shown in Supplementary Fig. 8, and source data for *(g)* and statistical source data and exact P values for *(e,h)* can be found in Supplementary Table 6. Unless otherwise noted, immunoblots are representative of three independent experiments.

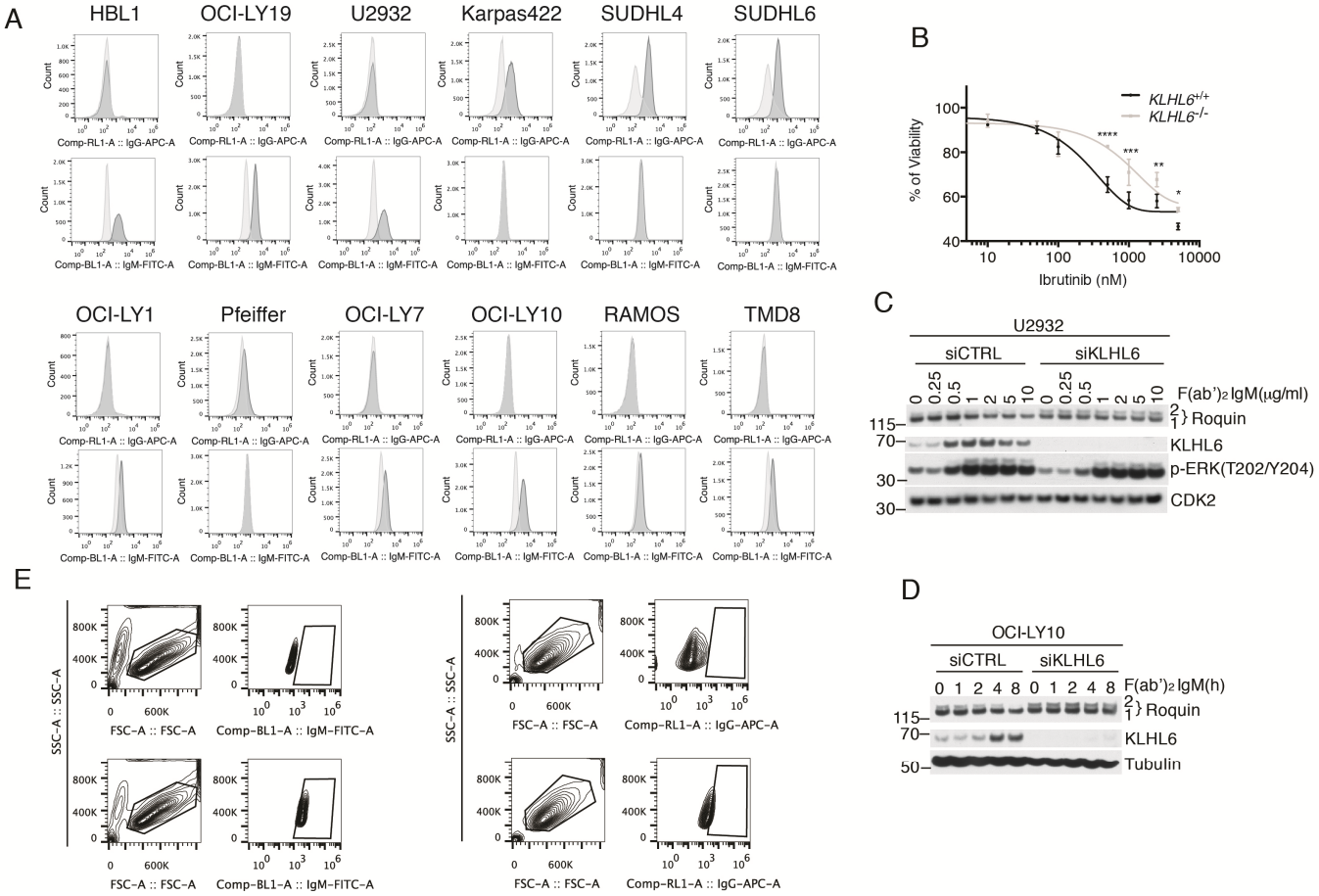

Supplementary Figure 5

Roquin2 is degraded upon BCR stimulation in a KLHL6-dependent manner.

(a) Flow cytometry analysis of a panel of human DLBCLs, as indicated, stained with anti-IgM or anti-IgG antibody to detect surface expression. A darker curve indicates a positive signal. A representative image from two independent experiments is shown. **(b)** MTS assay for U2932 cells *KLHL6*$^{+/+}$ and *KLHL6*$^{-/-}$ treated with increasing amounts of ibrutinib for 48 hours. Values were normalized to the non-treated cells and set as 100% (mean±s.d., n=3 independent experiments, two-way ANOVA; *P value≤0.05, **P value≤0.01, *** P value≤0.001, ****P value≤0.0001). **(c)** Immunoblot analysis of whole cell lysates from U2932 cells electroporated with a siRNA scramble (siCTRL) or siRNA targeting KLHL6 (siKLHL6) and treated with increasing concentrations of F(ab')2-IgM for 6 hours. **(d)** Immunoblot analysis of whole cell lysates from OCI-LY10 cells electroporated with siRNA scramble (siCTRL) or siRNA targeting KLHL6 (siKLHL6) and treated with 10μg/ml F(ab')2-IgM for the indicated times. **(e)** Gating strategy for *(a)*. The box indicates the stained cells. Unprocessed original scan of immunoblots for *(c,d)* are shown in Supplementary Fig. 8, and statistical source data and exact P values for *(b)* can be found in Supplementary Table 6. Unless otherwise noted, immunoblots are representative of three independent experiments.

A

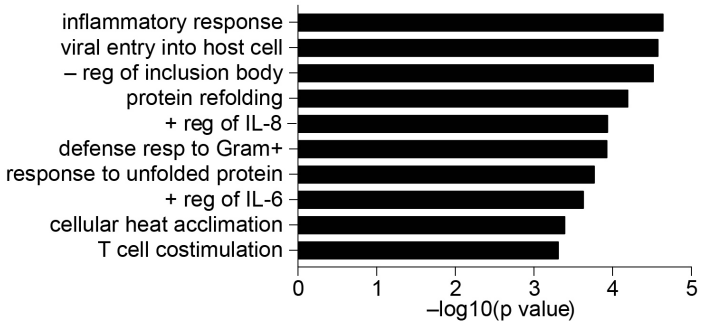

B

Gene	% Genetic Alteration	Base Mean	Rescue (>70%)
TNFAIP3	31%	1215.26	Yes
TNFRSF14	17%	733.84	Yes
TNF	15%	609.03	Yes
NFKBIE	13%	2832.97	No
LTA	10%	1609.40	Yes
NEDD4L	6%	14540.3	No
ABLIM1	6%	1958.09	No
SYNGAP1	6%	980.44	Yes
NEIL2	6%	253.09	Yes
LGALS8	6%	221.05	Yes
CD274	6%	152.22	No

C

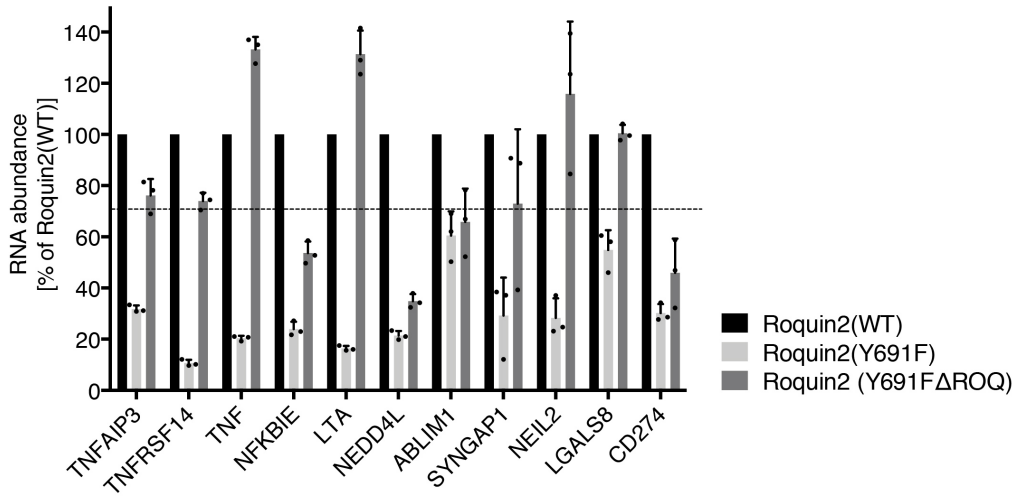

Supplementary Figure 6

Analysis of transcripts deregulated by non-degradable Roquin2(Y691F) mutant.

(a) Gene ontology (GO) analysis of genes regulated by the non-degradable Roquin2(Y691F) mutant. Bar plot for the $-\log_{10}$ of the *P* value of the top 10 enriched GO terms of genes regulated by Roquin2(Y691F) as determined by the hypergeometric distribution. -reg., negative regulation; + reg., positive regulation. Statistical analysis and genes list are provided in Supplementary Table 4. **(b)** Ranking of Roquin2-regulated genes by the percentage of genetic alteration in human DLBCLs from the TCGA database along with the base mean expression from the RNA-seq analysis. The cut-off was set at 6%. “Yes” indicates transcripts that are dependent on the ROQ domain of Roquin2; “No” indicates transcripts that are not dependent. **(c)** Level of indicated mRNAs analyzed by quantitative PCR from U2932 cells stably expressing HA-Roquin2(WT), HA-Roquin2(Y691F) or HA-Roquin2(Y691FΔROQ) and treated with 10μg/ml of F(ab’)2-IgM for 12 hours. The value for each PCR product present in HA-Roquin2(WT) cells was set as 100%. Rescued transcripts are defined as ones whose levels reach at least 70% of the Roquin2(WT) control (indicated by the dashed line) (mean±s.d., n=3 independent experiments). Source data for *(c)* can be found in Supplementary Table 6.

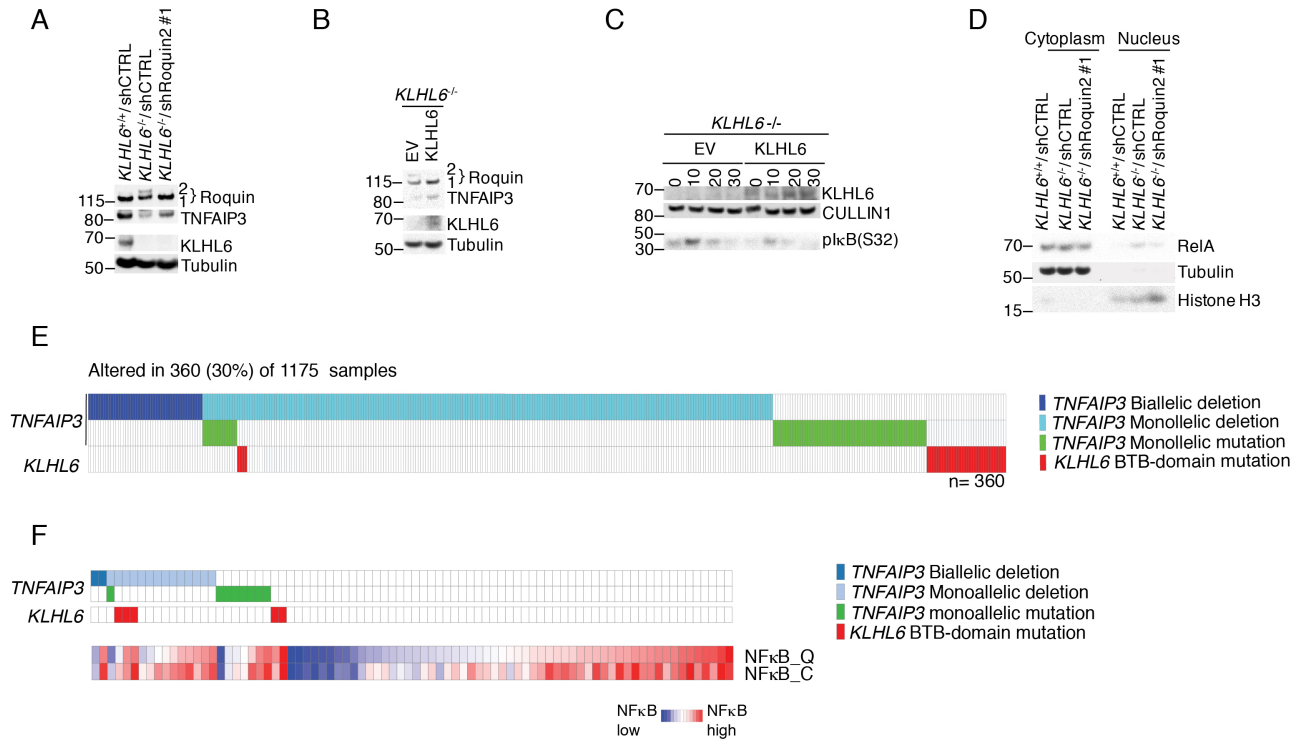

Supplementary Figure 7

KLHL6 regulates TNFAIP3 levels in a Roquin2-dependent manner.

(a) Immunoblot analysis of whole cell lysates from GFP-sorted U2932 *KLHL6*$^{+/+}$, *KLHL6*$^{-/-}$ or *KLHL6*$^{-/-}$ cells infected with lentiviruses encoding the indicated shRNAs carrying a GFP marker and treated with 10 μg/ml of F(ab')2-IgM for 6 hours. **(b)** Immunoblot analysis of whole cell lysates from GFP-sorted U2932 *KLHL6*$^{-/-}$ (clone-derived) cells infected with retroviruses encoding empty vector (EV) or KLHL6(WT) carrying a GFP marker and treated with 10μg/ml of F(ab')2-IgM for 6 hours. **(c)** Same as in *(b)* except that cells were treated with 10μg/ml F(ab')2-IgM for the indicated times (min). **(d)** GFP-sorted U2932 *KLHL6*$^{+/+}$, *KLHL6*$^{-/-}$ or *KLHL6*$^{-/-}$ cells infected with lentiviruses encoding the indicated shRNAs carrying a GFP marker were fractionated into cytoplasmic and nuclear extracts and analyzed by immunoblotting for the indicated proteins. **(e)** A heat map showing the presence of biallelic deletion (dark blue), monoallelic deletion (light blue) and monoallelic mutation (green) of *TNFAIP3* in DLBCL tumors sequenced at UNMC[6] and DCI[7] (n=1175). Deleterious mutations of *KLHL6* BTB-domain are shown in these same cases. Based on DCI database, exclusivity analysis of *KLHL6* and *TNFAIP3* mutations is provided in Supplementary Table 5 (n=1001). **(f)** A heat map showing tumor gene alterations matched with gene expression profiling data available at UNMC. Single sample gene set enrichment analysis (GSEA) was utilized to infer NF-κB activity via expression of target gene sets from the molecular signatures database (NFkB_Q and NFkB_C)[26,59]. The enrichment score is displayed as a row-normalized heat map. Unprocessed original scan of immunoblots for *(a,b,c,d)* are shown in Supplementary Fig. 8. Unless otherwise noted, immunoblots are representative of three independent experiments.